(12) INTERNATIONAL APPLICATION PUBLISHED UNDER THE PATENT COOPERATION TREATY (PCT)

(19) World Intellectual Property Organization
International Bureau

(43) International Publication Date
20 August 2020 (20.08.2020)

WIPO | PCT

(10) International Publication Number
WO 2020/164448 A1

(51) International Patent Classification:
C07D 215/06 (2006.01) *A61K 41/00* (2020.01)
C07D 209/82 (2006.01) *A61K 49/00* (2006.01)
C07D 209/88 (2006.01) *A61P 35/00* (2006.01)
C07D 401/06 (2006.01)

(21) International Application Number:
PCT/CN2020/074577

(22) International Filing Date:
10 February 2020 (10.02.2020)

(25) Filing Language: English

(26) Publication Language: English

(30) Priority Data:
62/918,750 12 February 2019 (12.02.2019) US

(71) Applicant: **THE HONG KONG UNIVERSITY OF SCIENCE AND TECHNOLOGY** [CN/CN]; Clear Water Bay, Kowloon, Hong Kong (CN).

(72) Inventors: **TANG, Benzhong**; c/o The Hong Kong University of Science and, Technology, Clear Water Bay, Kowloon, Hong Kong (CN). **ZHENG, Zheng**; c/o The Hong Kong University of Science and, Technology, Clear Water Bay, Kowloon, Hong Kong (CN).

(74) Agent: **TEE&HOWE INTELLECTUAL PROPERTY ATTORNEYS**; FAN, Xiaohuan, 10th Floor, Tower D, Minsheng Financial Center, 28 Jianguomennei Avenue, Dongcheng District, Beijing 100005 (CN).

(81) Designated States *(unless otherwise indicated, for every kind of national protection available)*: AE, AG, AL, AM, AO, AT, AU, AZ, BA, BB, BG, BH, BN, BR, BW, BY, BZ, CA, CH, CL, CN, CO, CR, CU, CZ, DE, DJ, DK, DM, DO, DZ, EC, EE, EG, ES, FI, GB, GD, GE, GH, GM, GT, HN, HR, HU, ID, IL, IN, IR, IS, JO, JP, KE, KG, KH, KN, KP, KR, KW, KZ, LA, LC, LK, LR, LS, LU, LY, MA, MD, ME, MG, MK, MN, MW, MX, MY, MZ, NA, NG, NI, NO, NZ, OM, PA, PE, PG, PH, PL, PT, QA, RO, RS, RU, RW, SA, SC, SD, SE, SG, SK, SL, ST, SV, SY, TH, TJ, TM, TN, TR, TT, TZ, UA, UG, US, UZ, VC, VN, WS, ZA, ZM, ZW.

(84) Designated States *(unless otherwise indicated, for every kind of regional protection available)*: ARIPO (BW, GH, GM, KE, LR, LS, MW, MZ, NA, RW, SD, SL, ST, SZ, TZ, UG, ZM, ZW), Eurasian (AM, AZ, BY, KG, KZ, RU, TJ, TM), European (AL, AT, BE, BG, CH, CY, CZ, DE, DK, EE, ES, FI, FR, GB, GR, HR, HU, IE, IS, IT, LT, LU, LV, MC, MK, MT, NL, NO, PL, PT, RO, RS, SE, SI, SK, SM, TR), OAPI (BF, BJ, CF, CG, CI, CM, GA, GN, GQ, GW, KM, ML, MR, NE, SN, TD, TG).

Published:
— *with international search report (Art. 21(3))*

WO 2020/164448 A1

(54) Title: Fluorescent Probes for Singlet Oxygen Generation and Cancer Ablation

(57) Abstract: A fluorescent probe can include a compound exhibiting near infrared (NIR) aggregation-induced emission (AIE). The probe can be used for the selective imaging and killing of cancer cells. The probe can specifically stain mitochondria and selectively target cancer cells over normal cells. The probe exhibits strong near-infrared (NIR) two-photon absorption (2PA), bright NIR emission and efficient singlet oxygen ($^1O_2$) generation. The probe can be used both in cancer cell-selective ablation and in in vivo melanoma therapy using image-guided PDT.

Fluorescent Probes for Singlet Oxygen Generation and Cancer Ablation

CROSS-REFERENCE

The present application claims priority to United States Provisional Patent Application No. 62/918,750, filed February 12, 2019, which was filed by the inventors hereof and is incorporated herein by reference in its entirety.

FIELD

The present subject matter relates generally to fluorescent probes which provide intense NIR emission, excellent NIR two-photon absorption, large Stokes shifts, superior mitochondria specificity and are efficient photosensitizers in photodynamic therapy.

BACKGROUND

Cancer is a well-recognized major public health problem and is likely to become even more of a leading cause of morbidity and mortality in the coming decades worldwide. As a typical example, malignant melanoma arising from melanocytes is the most dangerous form of skin cancer with a steeply rising incidence rate and a poor prognosis in its advanced stages due, in large part, to its propensity to metastasize. Once melanoma has spread beyond its original location, its treatment through a surgical process becomes extremely difficult, and it is usually highly resistant to traditional chemotherapy and radiotherapy.

As a promising alternative to chemotherapy and radiotherapy, photodynamic therapy (PDT) is emerging as an effective modality for cancer treatment because of its noninvasiveness, reduced side effects, negligible drug resistance, and low systemic toxicity. PDT relies on a photosensitizer (PS) and light to generate cytotoxic reactive oxygen species (ROS), particularly singlet oxygen ($^1O_2$), in the presence of oxygen to cause destruction of selected cells. As such, PDT has been approved in many countries for the treatment of lung, esophageal, bladder, skin and head and neck cancers.

Despite the advances in PDT, clinical application of PDT is still far from ideal due to the excess heating caused by use of strong lasers, and the intrinsic photo-toxicity and lack of selectivity of conventional PSs which can cause harmful side-effects on healthy tissues. While excess heating can be avoided by using light sources with low irradiation power, conventional PSs do not provide a sufficiently high therapeutic efficacy (efficient $^1O_2$ generation) that would be compatible with a low irradiation power.

The selectivity of PDT can be realized by employing PSs that are enriched more

completely in the tumorous tissue over healthy tissue. Moreover, a PS that targets a specific organelle, such as mitochondria, can be particularly useful because a singlet oxygen has a very short lifetime (<40 ns) and a small radius of action (<20 nm). Mitochondria are regarded as ideal target organelles for therapeutic applications because they are efficient in generating energy and mediating cell apoptosis. Thus, PSs with efficient $^1O_2$ generation, cancer cell selectivity and mitochondria-specific staining capability are crucial for improving PDT efficacy.

In addition, among diverse bioimaging techniques, fluorescence imaging has become a powerful tool for highly sensitive and noninvasive visualization of biological structures and processes in real time with high spatial resolution. Therefore, in terms of PS, the coupling of efficient $^1O_2$ generation with bright emission has been used for image-guided PDT. An ideal PS for image-guided PDT should provide bright near-infrared (NIR) emission (>700 nm), highly efficient $^1O_2$ generation, negligible dark toxicity, good photostability and biocompatibility.

While a number of organic NIR fluorophores such as porphyrin, chlorin, phthalocyanine and BODIPY derivatives have been recognized as PSs for image-guided PDT, these PSs often suffer from several intrinsic drawbacks, including small Stokes shift, low fluorescence quantum yield, moderate $^1O_2$ production, nonspecific targeting capability, poor photostability and unsatisfied biocompatibility. Further, these conventional PSs mostly possess rigid planar π-conjugation and are prone to aggregate in aqueous media which results in emission quenching or aggregation-caused quenching (ACQ) and insufficient $^1O_2$ production. As such, use of conventional PSs for image-guided PDT is problematic.

Aggregation-induced emission (AIE) was originally proposed in 2001 by Professor Ben Zhong Tang's group and the restriction of intramolecular motion (RIM) was identified as the main working mechanism behind the AIE phenomenon. AIE luminogens (AIEgens) are promising alternatives to traditional ACQ fluorophores for fluorescence imaging because of their higher emission brightness in aggregates, larger Stokes shift, superior photostability and great potential as "wash-free" and "light-up" probes.

More impressively, recent studies show that AIEgens could also efficiently generate $^1O_2$ in the aggregate, an important feature for image-guided PDT. However, many conventional AIE PSs display absorption and emission at short wavelengths. Development of AIE PSs with both absorption and emission in the NIR region is desirable for biological applications because they cause less photodamage, lower scattering, deeper light penetration, and better separation from

tissue autofluorescence. Further, a key parameter of AIE PSs is efficient $^1O_2$ generation. Therefore, an AIE PS with NIR excitation, bright NIR emission, efficient $^1O_2$ generation, cancer cell selectivity and mitochondria-specific staining capability for image-guided photodynamic anticancer therapy is highly desirable.

SUMMARY

The present subject matter relates to a fluorescent probe that can be used for the selective imaging and killing of cancer cells. The probes can specifically stain mitochondria and selectively target cancer cells over normal cells. The probes exhibit strong near-infrared (NIR) two-photon absorption (2PA), bright NIR emission and efficient singlet oxygen ($^1O_2$) generation. The probes can be used both in cancer cell-selective ablation and in *in vivo* melanoma therapy using image-guided PDT.

In an embodiment, the fluorescent probe comprises a compound having the following backbone structural formula:

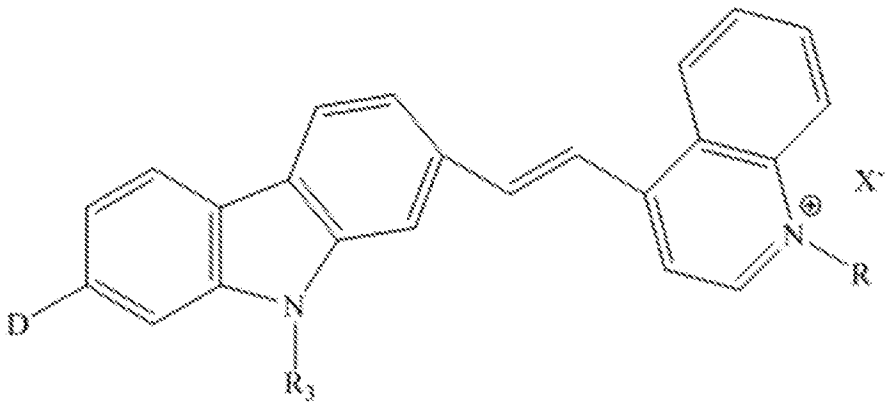

wherein each of R and R_3 is independently selected from the group consisting of H, alkyl, unsaturated alkyl, heteroalkyl, cycloalkyl, heterocycloalkyl, aryl, heteroaryl, alkoxy, alkyl-NCS, alkyl-N_3, and alkyl-NH_2;

X^- is selected from the group consisting of PF_6^-, BF_4^-, SbF_5^-, CH_3COO^-, CF_3COO^-, CO_3^{2-}, SO_4^{2-}, SO_3^{2-}, $CF_3SO_2^-$, TsO^-, ClO_4^-, F^-, Cl^-, Br^-, I^-, $(F_3CSO_2)N^-$, and PO_4^{3-};

D is selected from the group consisting of

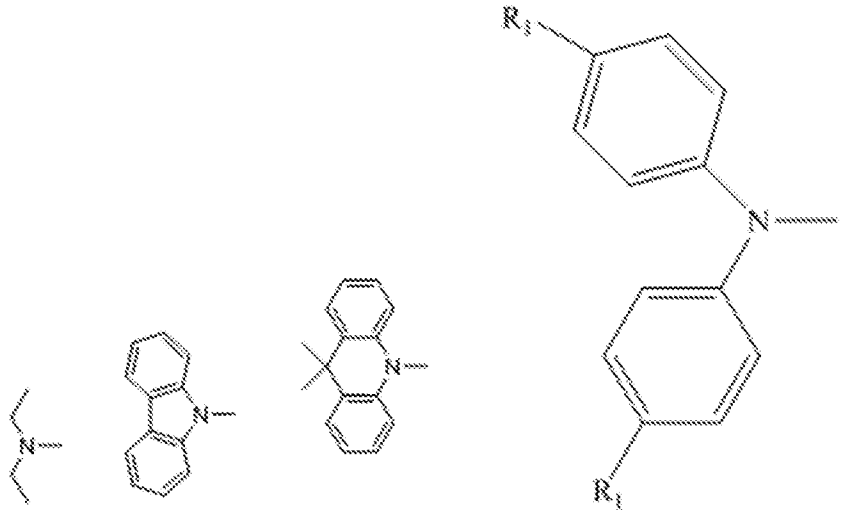
, , , , and

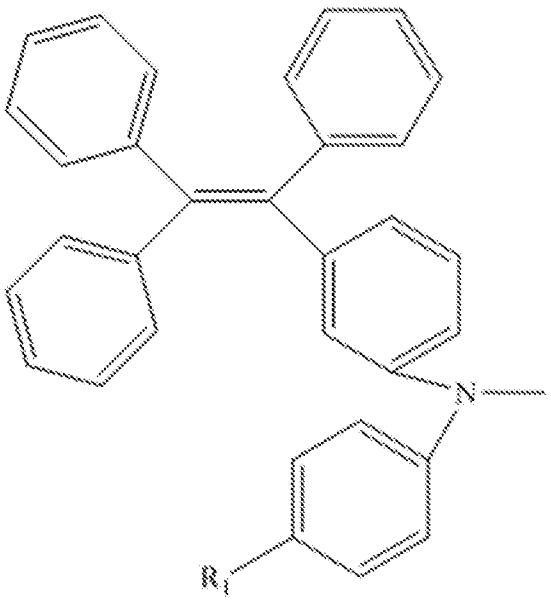
; and

each R_1 is independently selected from the group consisting of H, alkyl, unsaturated alkyl, heteroalkyl, cycloalkyl, heterocycloalkyl, aryl, heteroaryl, alkoxy, alkyl-NCS, alkyl-N_3, and alkyl-NH_2.

In an embodiment, the backbone structural formula is selected from the group consisting of:

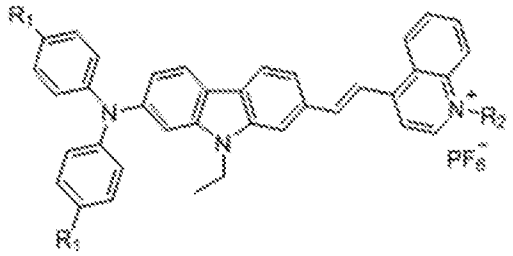

, and

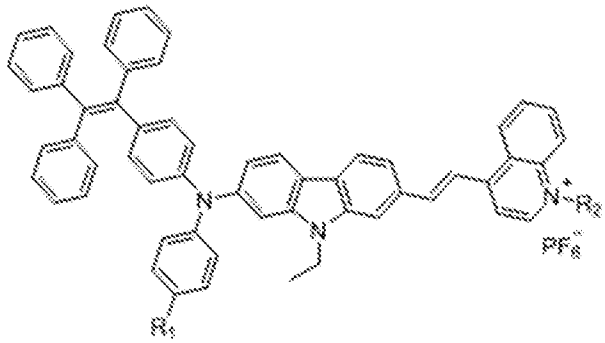

wherein each of R_1 and R_2 is independently selected from the group consisting of H, alkyl, unsaturated alkyl, heteroalkyl, cycloalkyl, heterocycloalkyl, aryl, heteroaryl, alkoxy, alkyl-NCS, alkyl-N_3, and alkyl-NH_2.

In an embodiment, the compound is:

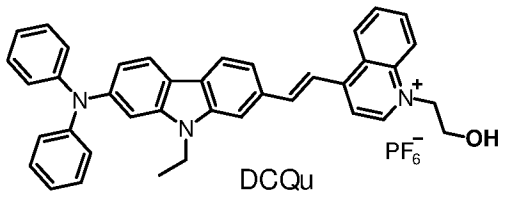

BRIEF DESCRIPTION OF DRAWINGS

Various embodiments will now be described in detail with reference to the accompanying drawings.

Figs. 1A-1E depict 1(A) absorption spectrum of DCQu in DMSO and PL spectrum of DCQu in the crystalline powder (Inset: Fluorescence photograph of DCQu crystal taken under fluorescence microscope); 1(B) PL spectra of DCQu (15 μM) in DMSO/toluene mixtures with different toluene fractions; λ_{ex} = 500 nm; 1(C) a plot of relative PL intensity (I/I_0) vs the composition of the DMSO/toluene mixtures of DCQu; 1(D) a two-photon absorption cross-section of DCQu ($c = 1 \times 10^{-4}$ M) in dioxane; and 1(E) (i) Single-crystal structure of DCQu, (ii) molecular stacking structures along the long molecule axis and (iii) the short molecule axis.

Fig. 2 depicts the molecular orbital amplitude plots of HOMO and LUMO levels of DCQu calculated at the B3LYP/6-31G based on the single-crystal structure.

Fig. 3 depicts fluorescence decay curves of DCQu in solid state.

Figs. 4A-4C depict 4(A) PL spectra of crystalline powder of DCQu at different input powers at 900 nm; 4(B) the corresponding linear relationship between the output fluorescence intensity and the square of input laser power (W^2); and 4(C) the two-photon excitation window of crystalline powder of DCQu.

Fig. 5A-5D depict fluorescent images of HeLa cells stained with 5(A) 0.1 μM concentration of DCQu; 5(B) 0.5 μM concentration of DCQu; 5(C) 1 μM concentration of DCQu; and 5(D) 5 μM concentration of DCQu, (where: 1 indicates 15 min. incubation time, 2 indicates 30 min. incubation time, and 3 indicates 60 min. incubation time; exposure time: 500 ms. Scale bar: 20 μm).

Fig. 6A-6C depict 6(A) (i) DCQu, (ii) MitoTracker Green, (iii) a merged image of i and ii, (iv) a scatter plot indicating a correction coefficient between panels i and ii; 6(B) fluorescence images of different normal cells (HLF and LX2) and cancer cells (HepG2, B16, A549 and HeLa) stained with DCQu (1 μM) for 30 min; and 6(C) relative fluorescence intensity of different cells incubated with DCQu (1 μM) for 30 min, the fluorescent intensity of these images was measured by Image J.

Fig. 7 is a graph depicting the extent of loss in fluorescence of HeLa cells stained with DCQu and MitoTracker Green with increasing number of sequential scans of laser irradiation (emission signal was normalized to the maximum intensity at the beginning of irradiation).

Figs. 8A-8B depict 8(A) two-photon excited fluorescence image (two-photon excitation wavelength: 900 nm) and 8(B) bright field of HeLa cells stained with DCQu (5 μm) for 30 min.

Figs. 9A-9F depict 9(A) absorption spectra of ABDA in the presence of DCQu under

white light (4.2 mW cm^{-2}) irradiation. [DCQu]: 5×10^{-6} M, [ABDA]: 5×10^{-5} M, time interval for UV measurement: 20 s; 9(B) decomposition rates of ABDA in the presence of different PSs under light irradiation, where A_0 and A are the absorbance of ABDA at 378 nm before and after irradiation. [PSs]: 5×10^{-6} M, [ABDA]: 5×10^{-5} M, time interval for UV measurement: 20 s; 9(C) images showing detection of intracellular ROS generation using H2DCF-DA in HeLa cells incubated with DCQu followed by irradiation with white light irradiation for a different time; 9(D) two-photon excited fluorescence (top row) and bright-field (bottom row) images of HeLa cells stained with DCQu (5 μM) followed by different two-photon (900 nm, fs Ti:sapphire laser) scans; 9(E) a graph showing cell viability of HeLa cancer cells and HLF normal cells stained with different concentrations of DCQu in the absence or presence of white light irradiation; and 9(F) a graph showing cell viability of melanoma cancer B16 stained with different concentrations of DCQu or Ce6 in the absence or presence of white light irradiation.

Fig. 10 depicts images showing detection of intracellular ROS generation using H2DCF-DA in HeLa cells incubated without DCQu followed by irradiation with white light irradiation for different lengths of time (Ex: 488 nm; Em: 580–740 nm).

Figs. 11A-11G depict 11(A) a diagram of in vivo PDT treatment of B16 melanoma-bearing mice with white light irradiation (4.2 mW cm^{-2}); 11(B) typical images of tumor tissues in mice upon completion of different groups of treatment protocols; 11(C) tumor growth curves of B16 melanoma-bearing mice for groups with different treatment protocols; 11(D) a graph showing calculated tumor inhibition ratios for each treating group; 11(E) a graph showing survival rate of mice upon different treatments; 11(F) a graph showing body weights of B16 melanoma-bearing mice in different groups during the whole treating period; and 11(G) histological sections of tumor tissues stained with hematoxylin and eosin.

Fig. 12 shows representative images of B16 melanoma-bearing mice in different groups during the treatment process.

Fig. 13 shows H&E-stained images of major organs of the mice after treating with light, free Ce6, free DCQu, Ce6 + light and DCQu + light (no noticeable abnormality was observed in major organs including heart, liver, spleen, lung, and kidney).

Fig. 14 shows crystal structure refinement for DCQu.

DETAILED DESCRIPTION

The following definitions are provided for the purpose of understanding the present subject matter and for construing the appended patent claims.

Definitions

It should be understood that the drawings described above or below are for illustration purposes only. The drawings are not necessarily to scale, with emphasis generally being placed upon illustrating the principles of the present teachings. The drawings are not intended to limit the scope of the present teachings in any way.

Throughout the application, where compositions are described as having, including, or comprising specific components, or where processes are described as having, including, or comprising specific process steps, it is contemplated that compositions of the present teachings can also consist essentially of, or consist of, the recited components, and that the processes of the present teachings can also consist essentially of, or consist of, the recited process steps.

In the application, where an element or component is said to be included in and/or selected from a list of recited elements or components, it should be understood that the element or component can be any one of the recited elements or components, or the element or component can be selected from a group consisting of two or more of the recited elements or components. Further, it should be understood that elements and/or features of a composition, an apparatus, or a method described herein can be combined in a variety of ways without departing from the spirit and scope of the present teachings, whether explicit or implicit herein

The use of the terms "include," "includes", "including," "have," "has," or "having" should be generally understood as open-ended and non-limiting unless specifically stated otherwise.

The use of the singular herein includes the plural (and vice versa) unless specifically stated otherwise. In addition, where the use of the term "about" is before a quantitative value, the present teachings also include the specific quantitative value itself, unless specifically stated otherwise. As used herein, the term "about" refers to a ±10% variation from the nominal value unless otherwise indicated or inferred.

It should be understood that the order of steps or order for performing certain actions is immaterial so long as the present teachings remain operable. Moreover, two or more steps or actions may be conducted simultaneously.

As used herein, "heteroaryl" refers to an aromatic monocyclic ring system containing at least one ring heteroatom selected from oxygen (O), nitrogen (N), sulfur (S), silicon (Si), and

selenium (Se) or a polycyclic ring system where at least one of the rings present in the ring system is aromatic and contains at least one ring heteroatom. Polycyclic heteroaryl groups include two or more heteroaryl rings fused together and monocyclic heteroaryl rings fused to one or more aromatic carbocyclic rings, non-aromatic carbocyclic rings, and/or non-aromatic cycloheteroalkyl rings. A heteroaryl group, as a whole, can have, for example, 5 to 22 ring atoms and contain 1 -5 ring heteroatoms (i.e., 5-20 membered heteroaryl group). The heteroaryl group can be attached to the defined chemical structure at any heteroatom or carbon atom that results in a stable structure. Generally, heteroaryl rings do not contain O—O, S—S, or S—O bonds. However, one or more N or S atoms in a heteroaryl group can be oxidized (e.g., pyridine N-oxide, thiophene S-oxide, thiophene S,S-dioxide). Examples of heteroaryl groups include, for example, the 5- or 6-membered monocyclic and 5-6 bicyclic ring systems shown below:

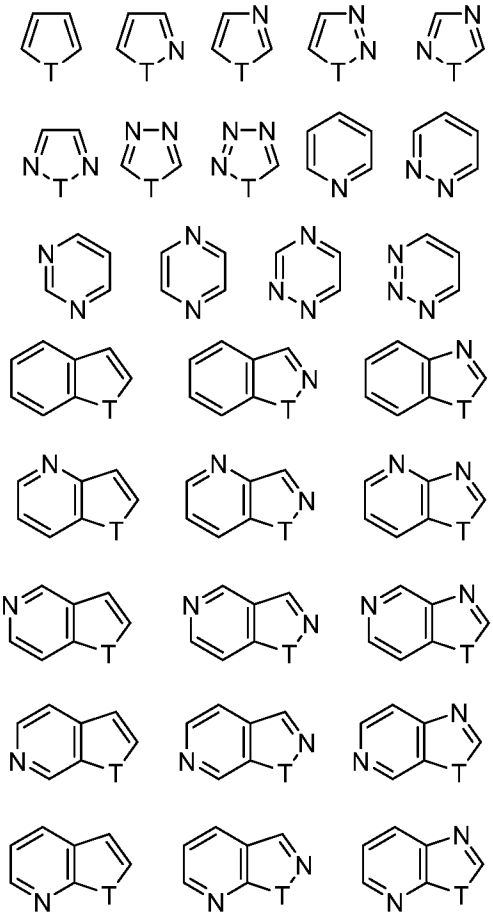

where T is O, S, NH, N-alkyl, N-aryl, N-(arylalkyl) (e.g., N-benzyl), SiH_2, SiH(alkyl), $Si(alkyl)_2$, SiH(arylalkyl), $Si(arylalkyl)_2$, or Si(alkyl)(arylalkyl). Examples of such heteroaryl rings include

pyrrolyl, furyl, thienyl, pyridyl, pyrimidyl, pyridazinyl, pyrazinyl, triazolyl, tetrazolyl, pyrazolyl, imidazolyl, isothiazolyl, thiazolyl, thiadiazolyl, isoxazolyl, oxazolyl, oxadiazolyl, indolyl, isoindolyl, benzofuryl, benzothienyl, quinolyl, 2-methylquinolyl, isoquinolyl, quinox-alyl, quinazolyl, benzotriazolyl, benzimidazolyl, benzothiazolyl, benzisothiazolyl, benzisoxazolyl, benzoxadiazolyl, benzoxazolyl, cinnolinyl, lH-indazolyl, 2H-indazolyl, indolizinyl, isobenzofuyl, naphthyridinyl, phthalazinyl, pteridinyl, purinyl, oxazolopyridinyl, thiazolopyridinyl, imidazopyridinyl, furopyridinyl, thienopyridinyl, pyridopyrimidinyl, pyridopyrazinyl, pyridopyridazinyl, thienothiazolyl, thienoxazolyl, thienoimidazolyl groups, and the like. Further examples of heteroaryl groups include 4,5,6,7-tetrahydroindolyl, tetrahydroquinolinyl, benzothienopyridinyl, benzofuropyridinyl groups, and the like. In some embodiments, heteroaryl groups can be substituted as described herein.

As used herein, "halo" or "halogen" refers to fluoro, chloro, bromo, and iodo.

As used herein, "alkyl" refers to a straight-chain or branched saturated hydrocarbon group. Examples of alkyl groups include methyl (Me), ethyl (Et), propyl (e.g., n-propyl and z'-propyl), butyl (e.g., n-butyl, z'-butyl, sec-butyl, *tert-butyl),* pentyl groups (e.g., n-pentyl, z'-pentyl, -pentyl), hexyl groups, and the like. In various embodiments, an alkyl group can have 1 to 40 carbon atoms (i.e., C1-40 alkyl group), for example, 1-30 carbon atoms (i.e., C1-30 alkyl group). In some embodiments, an alkyl group can have 1 to 6 carbon atoms, and can be referred to as a "lower alkyl group." Examples of lower alkyl groups include methyl, ethyl, propyl (e.g., n-propyl and z'-propyl), and butyl groups (e.g., n-butyl, z'-butyl, *sec-butyl, tert-butyl).* In some embodiments, alkyl groups can be substituted as described herein. An alkyl group is generally not substituted with another alkyl group, an alkenyl group, or an alkynyl group.

As used herein, "alkenyl" refers to a straight-chain or branched alkyl group having one or more carbon-carbon double bonds. Examples of alkenyl groups include ethenyl, propenyl, butenyl, pentenyl, hexenyl, butadienyl, pentadienyl, hexadienyl groups, and the like. The one or more carbon-carbon double bonds can be internal (such as in 2-butene) or terminal (such as in 1-butene). In various embodiments, an alkenyl group can have 2 to 40 carbon atoms (i.e., C2-40 alkenyl group), for example, 2 to 20 carbon atoms (i.e., C2-20 alkenyl group). In some embodiments, alkenyl groups can be substituted as described herein. An alkenyl group is generally not substituted with another alkenyl group, an alkyl group, or an alkynyl group.

As used herein, a "fused ring" or a "fused ring moiety" refers to a polycyclic ring system

having at least two rings where at least one of the rings is aromatic and such aromatic ring (carbocyclic or heterocyclic) has a bond in common with at least one other ring that can be aromatic or non-aromatic, and carbocyclic or heterocyclic. These polycyclic ring systems can be highly p-conjugated and optionally substituted as described herein.

As used herein, "heteroatom" refers to an atom of any element other than carbon or hydrogen and includes, for example, nitrogen, oxygen, silicon, sulfur, phosphorus, and selenium.

As used herein, "aryl" refers to an aromatic monocyclic hydrocarbon ring system or a polycyclic ring system in which two or more aromatic hydrocarbon rings are fused (i.e., having a bond in common with) together or at least one aromatic monocyclic hydrocarbon ring is fused to one or more cycloalkyl and/or cycloheteroalkyl rings. An aryl group can have 6 to 24 carbon atoms in its ring system (e.g., C6-24 aryl group), which can include multiple fused rings. In some embodiments, a polycyclic aryl group can have 8 to 24 carbon atoms. Any suitable ring position of the aryl group can be covalently linked to the defined chemical structure. Examples of aryl groups having only aromatic carbocyclic ring(s) include phenyl, 1-naphthyl (bicyclic), 2-naphthyl (bicyclic), anthracenyl (tricyclic), phenanthrenyl (tricyclic), pentacenyl (pentacyclic), and like groups. Examples of polycyclic ring systems in which at least one aromatic carbocyclic ring is fused to one or more cycloalkyl and/or cycloheteroalkyl rings include, among others, benzo derivatives of cyclopentane (i.e., an indanyl group, which is a 5,6-bicyclic cycloalkyl/aromatic ring system), cyclohexane (i.e., a tetrahydronaphthyl group, which is a 6,6-bicyclic cycloalkyl/aromatic ring system), imidazoline (i.e., a benzimidazolinyl group, which is a 5,6-bicyclic cycloheteroalkyl/aromatic ring system), and pyran (i.e., a chromenyl group, which is a 6,6-bicyclic cycloheteroalkyl/aromatic ring system). Other examples of aryl groups include benzodioxanyl, benzodioxolyl, chromanyl, indolinyl groups, and the like. In some embodiments, aryl groups can be substituted as described herein. In some embodiments, an aryl group can have one or more halogen substituents, and can be referred to as a "haloaryl" group. Perhaloaryl groups, i.e., aryl groups where all of the hydrogen atoms are replaced with halogen atoms *(e.g.,* -C_6F_5), are included within the definition of "haloaryl." In certain embodiments, an aryl group is substituted with another aryl group and can be referred to as a biaryl group. Each of the aryl groups in the biaryl group can be substituted as disclosed herein.

As used herein, a "theranostic agent" refers to an organic material having both diagnostic and therapeutic capabilities.

Unless defined otherwise, all technical and scientific terms used herein have the same meaning as commonly understood to one of ordinary skill in the art to which the presently described subject matter pertains.

Where a range of values is provided, for example, concentration ranges, percentage ranges, or ratio ranges, it is understood that each intervening value, to the tenth of the unit of the lower limit, unless the context clearly dictates otherwise, between the upper and lower limit of that range and any other stated or intervening value in that stated range, is encompassed within the described subject matter. The upper and lower limits of these smaller ranges may independently be included in the smaller ranges, and such embodiments are also encompassed within the described subject matter, subject to any specifically excluded limit in the stated range. Where the stated range includes one or both of the limits, ranges excluding either or both of those included limits are also included in the described subject matter.

Throughout the application, descriptions of various embodiments use "comprising" language. However, it will be understood by one of skill in the art, that in some specific instances, an embodiment can alternatively be described using the language "consisting essentially of" or "consisting of".

For purposes of better understanding the present teachings and in no way limiting the scope of the teachings, unless otherwise indicated, all numbers expressing quantities, percentages or proportions, and other numerical values used in the specification and claims, are to be understood as being modified in all instances by the term "about". Accordingly, unless indicated to the contrary, the numerical parameters set forth in the following specification and attached claims are approximations that may vary depending upon the desired properties sought to be obtained. At the very least, each numerical parameter should at least be construed in light of the number of reported significant digits and by applying ordinary rounding techniques.

Fluorescent Probes

The present subject matter relates to a fluorescent probe that includes a compound exhibiting near infrared (NIR) aggregation-induced emission (AIE). The compound can display bright NIR solid-state fluorescence centered at about 736 nm with a quantum yield of about 6%, a large Stokes shifts of about 218 nm and a large 2PA cross-section of up to about 795 GM. The compound exhibits specific mitochondria-targeting capability with good biocompatibility, high brightness and superior photostability. The compound can generate reactive oxygen species

(ROS) in photodynamic therapy (PDT) for both in vitro cancer cell-selective ablation and in vivo melanoma therapy. For example, the compound can be used as a photosensitizer in PDT to generate singlet oxygen ($^1O_2$) with a high efficiency.

In an embodiment, the compound can have the following backbone structural formula:

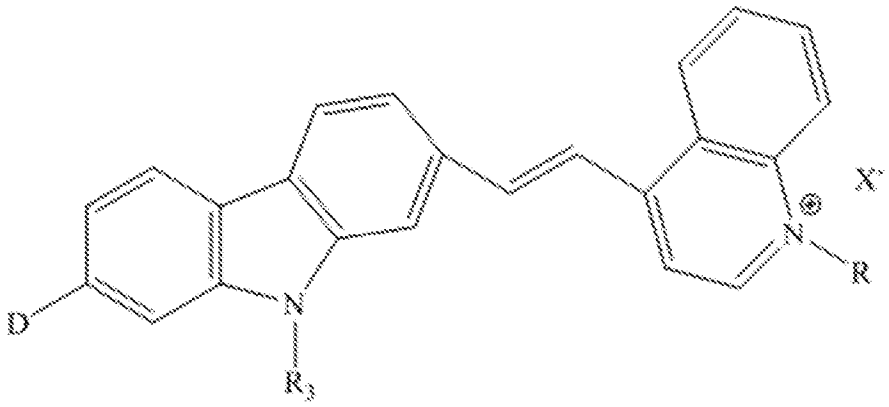

wherein each of R and R_3 is independently selected from the group consisting of H, alkyl, unsaturated alkyl, heteroalkyl, cycloalkyl, heterocycloalkyl, aryl, heteroaryl, alkoxy, alkyl-NCS, alkyl-N_3, and alkyl-NH_2;

X^- is selected from the group consisting of PF_6^-, BF_4^-, SbF_5^-, CH_3COO^-, CF_3COO^-, CO_3^{2-}, SO_4^{2-}, SO_3^{2-}, $CF_3SO_2^-$, TsO^-, ClO_4^-, F^-, Cl^-, Br^-, I^-, $(F_3CSO_2)N^-$, and PO_4^{3-};

D is selected from the group consisting of

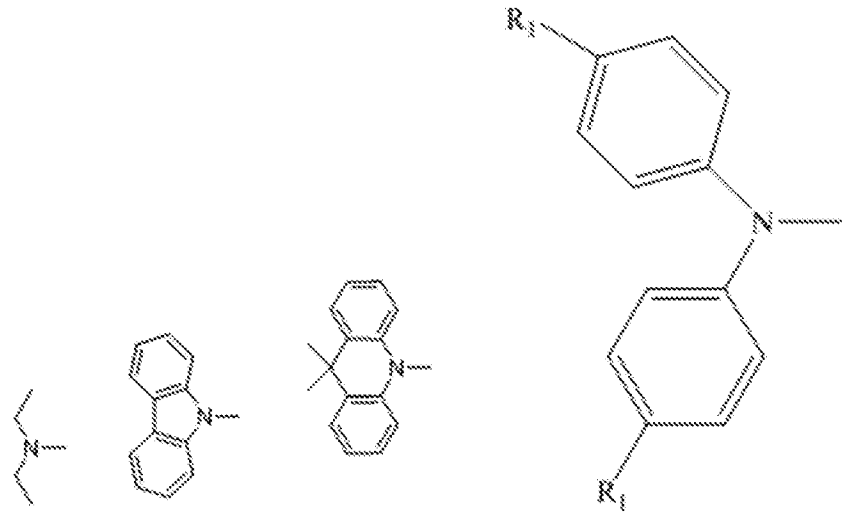

, , , , and

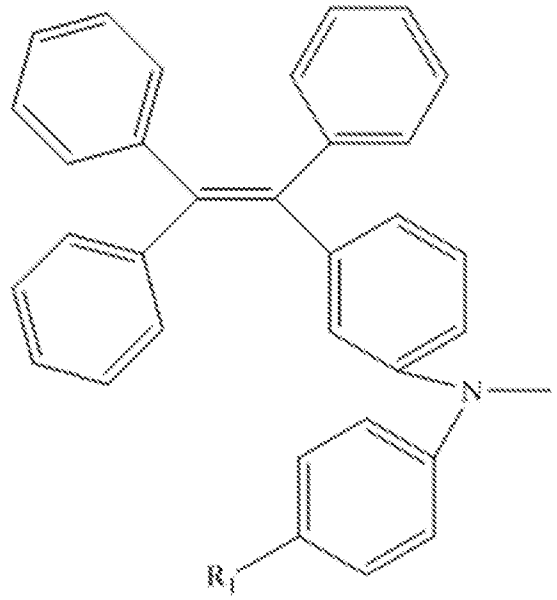

; and

each R_1 is independently selected from the group consisting of H, alkyl, unsaturated alkyl, heteroalkyl, cycloalkyl, heterocycloalkyl, aryl, heteroaryl, alkoxy, alkyl-NCS, alkyl-N_3, and alkyl-NH_2.

In a further embodiment, the backbone structural formula is selected from the group consisting of

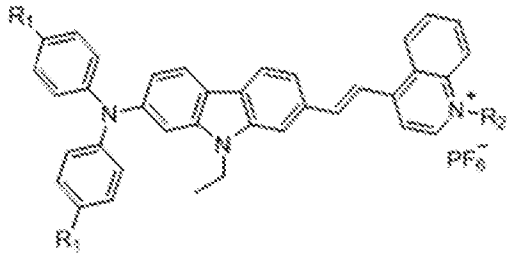

and

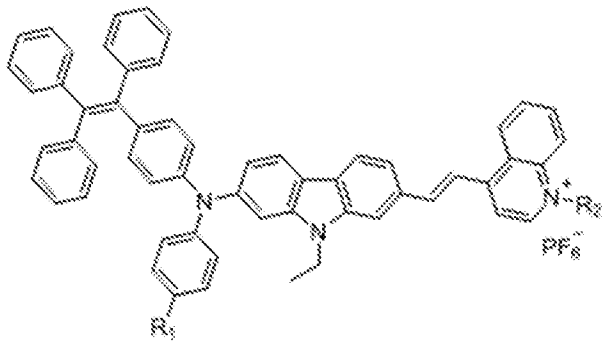

,

wherein each of R_1 and R_2 is independently selected from the group consisting of H, alkyl, unsaturated alkyl, heteroalkyl, cycloalkyl, heterocycloalkyl, aryl, heteroaryl, alkoxy, alkyl-NCS, alkyl-N_3, and alkyl-NH_2.

In an embodiment, the compound is:

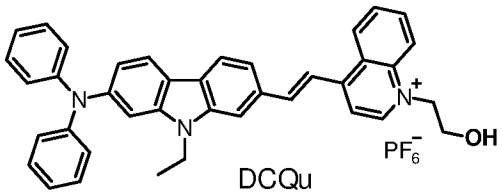

.

Selectively Identifying Cancer Cells and Stopping Cell Growth

As set forth in detail herein, imaging studies demonstrate that the present compounds can serve as an effective probe to selectively identify cancer cells. The present compounds can selectively target cancer cells over normal cells. In particular, the present compounds can stain the mitochondria of cancer cells with high brightness and high signal-to-noise ratio.

Once cancer cells have been identified, the compounds can be exposed to white light, causing the compounds to act as photosensitizers. The present compounds can provide extremely high reactive oxygen species, e.g., singlet oxygen, generation efficiency upon exposure to white light irradiation. The present compounds can, thereby, provide selective cytotoxicity to the cancer cells. In an embodiment, the present compounds can be used for in vitro cancer cell-selective ablation. The present compounds can be effective photosensitizers in image-guided

PDT. In an embodiment, the present compounds can be used as photosensitizers for in vivo melanoma PDT.

In an embodiment, a method of cellular imaging can include contacting a target cell with the fluorescent compound and identifying a cellular target of interest using an imaging method. The imaging method can include at least one of fluorescence microscopy and confocal laser scanning microscopy. The fluorescence microscopy can include at least one of one-photon fluorescence microscopy and two-photon fluorescence microscopy. In an embodiment, the target of interest can include a mitochondrion of the target cell.

In an embodiment, a method of killing cancer cells can include contacting a target cancer cell with the fluorescent compound, imaging the target cancer cell while the compound contacts the target cancer cell using an imaging method, and subjecting the target cancer cell to white light irradiation while the compound is contacting the target cancer cell to kill the target cancer cell. In an embodiment, subjecting the target cancer cell to white light irradiation can include using an ultralow-power lamp having an irradiation power of about 4.2 mW cm^{-2}. In an embodiment, the target cancer cell is within a living animal. In an embodiment, the target cancer cell is a melanoma cancer cell.

As the present compounds are completely organic, these compounds show good biocompatibility, and no detectable side toxicity. The compounds demonstrate ultra-high stability and good photodynamic performance, making them promising candidates for diagnosis and therapy applications.

The present teachings are illustrated by the following examples.

EXAMPLES

Materials and Instruments

All chemicals and reagents were commercially available and used as received without further purification. The intermediates 1-(2-hydroxyethyl)-4-methylquinolinium iodide and 7-(diphenylamino)-9-ethyl-9H-carbazole-2-carbaldehyde were synthesized following known procedures. 9,10-Anthracenediyl-bis(methylene)dimalonic acid (ABDA), 2',7'-dichlorodihydrofluorescein diacetate (H2DCF-DA) and 3-(4,5-dimethyl-2-thiazolyl)-2,5-diphenyltetrazolium bromide (MTT) were purchased from Sigma-Aldrich and used as received. For cell culture, minimum essential medium (MEM), fetal bovine serum (FBS), penicillin-

streptomycin solution, MitoTracker Green FM were purchased from Invitrogen.

Characterization

^{1}H and ^{13}C NMR spectra were measured on a Bruker ARX 400 NMR spectrometer using $CDCl_3$ and DMSO-d_6 as solvents and tetramethylsilane (TMS; $\delta = 0$ ppm) was chosen as internal reference. High-resolution mass spectra (HR-MS) were obtained on a Finnigan MAT TSQ 7000 Mass Spectrometer System operated in a MALDI-TOF mode. Absorption spectra were measured on a Milton Roy Spectronic 3000 Array spectrophotometer. Steady-state photoluminescence (PL) spectra were measured on a Perkin-Elmer spectrofluorometer LS 55. Absolute fluorescence quantum yield was measured by a calibrated integrating sphere (Labsphere). Single crystal data was collected on a SuperNova, Dual, Cu at zero, Atlas diffractometer. The crystal was kept at 100.01(10) K during data collection. Using Olex2, the structure was solved with the Superflip structure solution program using Charge Flipping and refined with the ShelXL refinement package using Least Squares minimisation. Two-photon excitation fluorescence cross-section was measured by the two-photon excitation fluorescence method using rhodamine B as reference. The excitation source for two-photon excitation was a femtosecond optical parametric amplifier (Coherent OPerA Solo) pumped by an amplified Ti:Sapphire system (Coherent Legend Elite system) and then detected with a spectrometer (Acton SpectraPro-500i) coupled to a CCD. Simulation was carried out with the Gaussian 09 package. Laser confocal scanning microscope images were collected on a Zeiss laser scanning confocal microscope (LSM710) and analyzed using ZEN 2009 software (Carl Zeiss).

Cell Culture

Cell lines were cultured in MEM containing 10% FBS and antibiotics (100 units per mL penicillin and 100 μg/mL streptomycin) in a 5% CO_2 humidity incubator at 37 °C.

Cytotoxicity of DCQu to cells under light irradiation

Cytotoxicity was evaluated by 3-(4,5-Dimethythiazol-2-yl)-2,5-diphenyltetrazolium bromide (MTT) assays in accordance with the manufacturer's manual. Cells were seeded in 96-well plates (Costar, IL, USA) at a density of 6000–8000 cells per well. After overnight culturing, medium in each well was replaced by 100 μL fresh medium containing different concentrations of DCQu or Ce6. The volume fraction of DMSO was below 0.2%. After incubation for 30 min, plates containing cells with fresh medium were exposed to white light (4.2 mW/cm^{-2}) for 90 min and another array of plates with cells was kept in the dark as a control.

Then, the plates were subjected to the same treatment as the biocompatibility test. After 24 h, 10 μL of MTT solution (5 mg/mL in PBS) was added into each well. After 4 h incubation, DMSO was added into each well and the plate was gently shaken to dissolve all of the precipitate formed. Finally, the absorption of each well at 570 nm was recorded *via* a plate reader (Perkin-Elmer Victor3TM). Each trial was performed with five wells parallel.

Cell imaging

Cells were grown in a 35-mm petri dish with a cover slip. The cells were stained with a certain dye at a certain concentration (by adding 2 μL of stock solution in DMSO to a 2 mL of MEM with DMSO < 0.1 vol %) for 30 min. For co-staining with MitoTracker Green, cells were first incubated with DCQu and MitoTracker Green (0.5 μM) at 37 °C for 30 min. After incubation with the dye, the cells were washed with PBS three times. The cells were imaged under a confocal microscope (Zeiss LSM 710 Laser Scanning Confocal Microscope), using proper excitation and emission filters for each dye: for DCQu, excitation filter = 488 nm and emission filer = 600–740 nm; for MitoTracker Green, excitation filter = 488 nm and emission filter = 500–530 nm.

Two-photon fluorescence imaging in cells

HeLa cells used for two-photon microscopy were stained with DCQu (5 μM) in accordance with the procedure described for confocal fluorescence imaging. Two-photon fluorescence images of HeLa cells were collected using a Stimulated Emission Depletion (STED) microscopy (Leica Stimulated Emission Depletion Microscope) equipped with a multiphoton laser (Coherent Chameleon Ultra II Multiphoton laser). Excitation wavelength = 900 nm; emission filter = 600–740 nm.

Two-photon PDT

HeLa cells were seeded in a 2×10^5 / confocal image dish with 2 mL DMEM medium supplied with 10% FBS and 1% PLS. After 24 hours, cells were stained with 5 μM DCQu for 30 min at 37 ℃, and then kept with fresh medium. Cells were then imaged under STED microscope equipped with two-photon laser with 900 nm excitation, 2500 W (67% gain). Images were taken after 1, 2, 4, 8, 16 and 32 scans.

Photostability

The Hela Cells labelled with certain dyes were imaged by a confocal microscope (Zeiss LSM 710 Laser Scanning Confocal Microscope). The dyes were excited with 488 nm laser light

for one-photon imaging. Imaging parameters were set for each dye individually to obtain optimal images. Continuous scans (11s per Scan) were taken. For each series of scans, three regions of interest (ROIs) with mitochondria were defined. The first scan of each ROI was set to 100%. Then the pixel intensity values for each ROI were averaged and plotted against the scan number. The resulting curve represented the bleaching rate that an experimentalist would encounter.

Example 1

Synthesis of DCQu

To start the synthesis of DCQu, the precursor 7-(diphenylamino)-9-ethyl-9H-carbazole-2-carbaldehyde was initially obtained in two steps starting from ethylation of 2,7-dibromo-9-ethyl-9H-carbazole, followed by formylation reaction under acidic conditions. The single crystal of the intermediate aldehyde was obtained and analyzed by X−ray crystallography . The crystal data is provided in Table 1.

Table 1. Crystal data and structure refinement for intermediate aldehyde.

Identification code	zhengz1a
Empirical formula	$C_{27}H_{22}N_2O$
Formula weight	390.46
Temperature/K	100.01(10)
Crystal system	Monoclinic
Space group	$P2_1/n$
a/Å	9.53897(10)
b/Å	23.1410(2)
c/Å	9.57210(10)
α/°	90
β/°	107.3297(12)
γ/°	90
Volume/Å^3	2017.04(4)
Z	4
ρ_{calc}g/cm^3	1.286
μ/mm^{-1}	0.613
F(000)	824.0
Crystal size/mm^3	0.3 × 0.3 × 0.25
Radiation	CuKα (λ = 1.54184)
2Θ range for data collection/°	7.64 to 134.97
Index ranges	$-11 \leq h \leq 11$, $-27 \leq k \leq 27$, $-11 \leq l \leq 7$
Reflections collected	10527
Independent reflections	3583 [R_{int}= 0.0108, R_{sigma}= 0.0110]
Data/restraints/parameters	3583/0/281
Completeness to theta = 66.5°	98.4%
Goodness-of-fit on F^2	1.001
Final R indexes [I>=2σ (I)]	R_1= 0.0349, wR_2= 0.0958
Final R indexes [all data]	R_1= 0.0360, wR_2= 0.0967
Largest diff. peak/hole / e Å^{-3}	0.20/-0.17

Knoevenagel condensation of the precursor aldehyde with active methyl quinolinium in ethanol followed by anion exchange to replace iodide with hexafluorophosphate gave rise to DCQu in an excellent yield of 79%. An exemplary reaction scheme for preparing the DCQu compound is provided below:

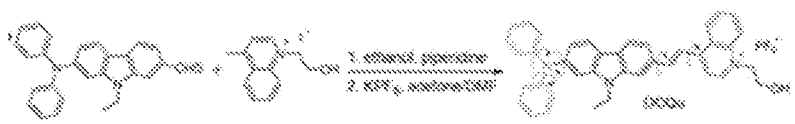

7-(diphenylamino)-9-ethyl-9H-carbazole-2-carbaldehyde (0.5 g, 1.28 mmol) and 1-(2-hydroxyethyl)-4-methylquinolinium iodide (0.37 g, 1.16 mmol) were dissolved in dry ethanol (15 mL). 2 drops of piperidine was added and the solution was refluxed for 3 h under nitrogen. After cooling to room temperature, the precipitated solid was filtered, washed with cold ethanol and dried to give the iodide salt of the product as a purple solid (0.62 g, yield: 78%). Then, the solid was dissolved in acetone (20 mL) and a saturated aqueous solution of KPF_6 (20 mL) was then added. After stirring for 30 min, the solution was evaporated to dryness. The residue was purified by flash silica gel column chromatography eluting with dichloromethane/methanol (20:1, v:v) giving DCQu as purple crystalline solid (0.63 g, yield: 99%). ^{1}H NMR (400 MHz, DMSO-d_6, ppm): δ 9.20 (d, J = 6.6 Hz, 1H), 9.11 (d, J = 8.4 Hz, 1H), 8.55 (d, J = 9.0 Hz, 1H), 8.51 (d, J = 6.6 Hz, 1H), 8.45 (d, J = 15.9 Hz, 1H), 8.35 (d, J = 15.8 Hz, 1H), 8.25-8.22 (m, 2H), 8.17 (d, J = 8.1 Hz, 1H), 8.10-8.03 (m, 2H), 7.81 (d, J = 7.8 Hz, 1H), 7.33-7.29 (m, 4H), 7.18 (s, 1H), 7.08-7.03 (m, 6H), 6.87 (dd, J = 8.4 Hz, 1.7 Hz, 1H), 5.19 (t, J = 5.6 Hz, 1H), 5.04 (t, J = 4.5 Hz, 2H), 4.36 (q, J = 6.2 Hz, 2H), 3.93 (q, J = 4.8 Hz, 2H), 1.27 (t, J = 7.1 Hz, 3H). ^{13}C NMR (100 MHz, DMSO-d_6, ppm): δ 152.96, 147.91, 147.35, 146.67, 144.61, 141.77, 140.12, 137.99, 134.70, 132.12, 129.36, 128.83, 126.59, 126.54, 124.51, 123. 63, 122.83, 121.86, 120.76, 120.32, 120.02, 118.22, 117.59, 116.68, 115.30, 109.03, 104.03, 58.79, 58.64, 36.84, 13.55. HRMS (MALDI-TOF): m/z calcd. for $C_{39}H_{34}N_3O$ $[M\text{-}PF_6]^+$: 560.2696, found: 560.2714.

Example 2

Photophysical Properties of DCQu

The target compound was fully characterized by NMR, high resolution mass spectrometry and single crystal X−ray diffraction analyses (Table 2). The data obtained was in good agreement with the proposed structure.

Table 2. Crystal data and structure refinement for DCQu.

Identification code	DCQu
Empirical formula	$C_{39}H_{34}F_6N_3OP$
Formula weight	705.66
Temperature/K	100.01(10)
Crystal system	Monoclinic
Space group	$P2_1/c$
a/Å	9.3923(3)
b/Å	29.4208(8)
c/Å	11.9664(3)
α/°	90
β/°	102.511(3)
γ/°	90
Volume/Å^3	3228.14(16)
Z	4
ρ_{calc}g/cm^3	1.452
μ/mm^{-1}	1.390
F(000)	1464.0
Crystal size/mm^3	0.25 × 0.2 × 0.05
Radiation	CuKα (λ = 1.54184)
2Θ range for data collection/°	8.144 to 152.372
Index ranges	$-11 \leq h \leq 11$, $-36 \leq k \leq 23$, $-14 \leq l \leq 9$
Reflections collected	10260
Independent reflections	6341 [R_{int}= 0.0209, R_{sigma}= 0.0334]
Data/restraints/parameters	6341/0/453
Completeness to theta = 66.5°	98.1%
Goodness-of-fit on F^2	1.026
Final R indexes [I>=2σ (I)]	R_1= 0.0650, wR_2= 0.1706
Final R indexes [all data]	R_1= 0.0750, wR_2= 0.1803
Largest diff. peak/hole / e Å^{-3}	0.98/-0.52

The photophysical properties of DCQu were subsequently investigated by UV–vis absorption and photoluminescence (PL) spectra. As depicted in Fig. 1A, DCQu shows a broad absorption in dimethyl sulfoxide (DMSO) with a maximum peak centered at 507 nm, which is attributed to intramolecular charge transfer (ICT) transition from the electron-donating diphenylamino group to the electron-accepting quinolinium group. To better understand the ICT transitions within molecules, density functional theory (DFT) calculation was performed for DCQu by using the single-crystal structure determined by X–ray analysis (Fig. 2). The electron clouds of the HOMO is mainly located on the diphenylamino moiety and the central carbazole ring, whereas the LUMO level is primarily localized on the acceptor framework, suggesting a strong charge transfer characteristics within the fluorophore.

The AIE property of DCQu was then studied in DMSO/toluene mixtures with different

toluene fractions. (Figs. 1B and 1C). In pure DMSO, DCQu showed a negligible emission, which was mainly caused by energy consumption of the excited state through nonradiative pathways owing to the strong molecular rotations in the solution state. Upon increasing the toluene fraction, the fluorescence intensities of the compound in the mixture solvent were gradually boosted with 243-fold enhancement, resulting from the restriction of rotational motions caused by the formation of aggregates. These results reveal that DCQu is AIE active in the NIR region, with the maximum emission located at 725 nm. Owing to the AIE characteristics, DCQu showed a bright NIR solid state fluorescence peaked at 736 nm with the fluorescence quantum yield (Φ_f) of 6% determined by the integrating sphere. Time-resolved fluorescence measurements for DCQu in the solid state reveal that its lifetime is 1.34 ns (Fig. 3). Moreover, DCQu exhibited a very large Stokes Shift of 218 nm, which is favorable for bio-imaging applications due to the minimized interference between excitation and emission.

The strong push–pull dipolar character as well as the extended conjugation of DCQu was expected to endow the molecule with 2PA properties. Thus, the two-photon excitation spectra of DCQu was first recorded in dioxane using the two-photon-excited fluorescence (TPEF) method. The emission signals were collected upon excitation from 800 to 1040 nm (at 40 nm intervals), in which compounds have no linear absorption. As shown in Fig. 1D, DCQu displayed excellent 2PA activity in the range of 800–1040 nm with a maximum 2PA cross-section (σ_{2P}) of 795 GM at 1000 nm. Moreover, the σ_{2P} values of the synthesized carbazole-bridged push–pull fluorophores were greatly improved compared to the previously reported values for phenyl-bridged AIEgens and other fluorophores.

In view of the strong solid state fluorescence, the two-photon-excited fluorescence of DCQu in the solid state was also investigated (Figs. 4A-4C). Upon excitation by 900 nm laser light, the upconversion PL spectra of DCQu in the solid state exhibited a similar emission maximum as the one-photon measurement, which illustrates that the emission processes from the one- and two-photon excited states to the ground state are the same. When the power of the excitation source was increased, the two-photon-excited fluorescence intensity showed a square dependence with the incident energy, implying that the upconverted emission stems from a two-photon absorption process. Similar to DCQu in solution, DCQu in the solid state also presents a broad two-photon excitation window ranging between 800 and 1040 nm. These results strongly demonstrate the design of the conjugated dipolar chromophores for achieving good 2PA activity

located at a biological transparency window in the range of 700–1000 nm.

Example 3

Crystal Structure

After observing the AIE effect and bright NIR solid state fluorescence of DCQu, its molecular conformation and molecular arrangement in crystal structure were investigated. Crystals suitable for single crystal X–ray analysis were obtained by slow evaporation from ethanol/CH_2Cl_2 mixture solution. The crystal data and collection parameters are summarized in Table 2, above. DCQu crystallized in the monoclinic $P2_1/c$ space group with an elemental cell containing four molecules. Single crystal X–ray diffraction analyses provided direct evidence for the absolute structure of DCQu, in particular the *trans*-conformation. The crystal structure revealed that the carbazole and quinolinium moieties are essentially planar and conjugated manifested by their small dihedral angle of 1.65°, allowing good π-electron delocalization over the whole molecule.

Thus, the strong push–pull character in combination with the extended π-conjugation within the fluorophore not only effectively shifts emission wavelength to NIR but also can dramatically improve nonlinear optical properties, which are perfectly consistent with its NIR emission and excellent two-photon property. As shown in Fig. 1F, the planar molecules further arrange into offset columnar stacks of antiparallel dimers along the long molecular axis with a slip angle of 45.8°, revealing a *J*-type packing through close intermolecular π–π stacking. Crystal packing diagrams of DCQu show that multiple inter- and intramolecular interactions, such as P–F···H, C–H···π and π···π interactions, help rigidify the molecular conformation and lock the intramolecular rotations. Thus, the excited-state energy consumed by intramolecular rotation is greatly reduced in the solid state, enabling the molecules to emit intense NIR fluorescence with AIE characteristic.

Example 4

One- and Two-Photon Bioimaging

The integration of strong NIR 2PA, NIR AIE characteristics and large Stokes shift makes DCQu a promising candidate for biological applications. Cell imaging experiments were initially conducted by incubating HeLa cells with different concentrations of DCQu for 15, 30 and 60 min, followed by observation under an excitation of 488 nm. As shown in Figs. 5A-5D, both

concentration and incubation time have an obvious influence on cell imaging. For the same incubation time, the fluorescence signal is gradually increased with increasing DCQu concentration. For the same concentration of DCQu, the fluorescence signal was enhanced with the extension of culture time from 15 min. to 30 min. Further increasing culture time to 60 min. did not cause an obvious difference in fluorescence signal. Notably, the fluorescence of DCQu was still observed in cells incubated with a DCQu concentration as low as 0.1 μM, suggesting a high brightness of DCQu in cell imaging.

To further realize the specificity of the AIEgens for cell imaging, colocalization experiments were then carried out by incubating HeLa cells with DCQu and then MitoTracker Green, which is a commercially available probe for mitochondria. As shown in Fig. 6A (iii), the image stained with DCQu (i) perfectly overlapped with that of MitoTracker Green (ii), giving rise to a high Pearson's correlation coefficient of 0.95 (iv), and indicating the superior specificity of DCQu for mitochondria staining.

The mitochondria-specific targeting capability of the cationic lipophilic DCQu mainly relies on the driven force of a very large membrane potential of around 180 mV across the mitochondrial membrane. Photostability of DCQu, as a key criterion for evaluating a fluorescent bioprobe, was subsequently checked by continuous laser excitation and sequential scanning with confocal microscope. As illustrated in Fig. 7, the fluorescence intensity of MitoTracker Green faded to 89% of its initial value during 60 scans. In comparison, for DCQu, its fluorescence signal slightly decreased to 92% of its initial value during the same process, displaying a superior photostability compared with the commercial dye.

The applicability of DCQu for two-photon imaging of mitochondria was also conducted. As shown in Figs. 8A-8B, DCQu clearly stains the mitochondria within HeLa cells under two-photon excitation at 900 nm, revealing a promising candidate as a two-photon imaging probe for achieving NIR-to-NIR imaging of mitochondria in living cells.

Cancer cells generally possess a more negatively charged surface than normal cells because positive ions on the cancer cell surface can be removed by the secreted lactate anions generated by the higher level of lactate secretion in the elevated glycolysis inside the cancer cells. In addition, the more active metabolism of cancer cells shows a higher mitochondrial membrane potential (MMP) than normal cells with a difference of at least 60 mV. This unique electrostatic pattern on the cancer cell membrane as well as the mitochondrial membrane has

been proven to be a powerful driving force for discriminating cancer cells over normal cells through the strong electrostatic interaction with a positively charged object.

After the intrinsic positive charge and mitochondria-specific capability of DCQu were determined, the ability of DCQu to differentiate between cancer cells and normal cells was investigated. Various cancer cells and normal cells were incubated with DCQu under the same conditions followed by observation under confocal fluorescence microscopy. As illustrated in Figs. 6B and 6C, DCQu is more prone to accumulate in cancer cells, including HepG2, B16, A549 6B and HeLa, and stain mitochondria with high brightness and high signal-to-noise ratio. By contrast, normal cells such as HLF and LX2 display a much weaker fluorescence. These results demonstrated a promising capability of DCQu for selectively targeting cancer cells without using any molecular biomarkers.

Example 5

Photodynamic therapy

The PDT application of DCQu was subsequently investigated. Considering DCQu has strong absorption in the visible light region, the $^1O_2$ generation ability of DCQu was initially evaluated using ultralow-power white light irradiation (400–700 nm, 4.2 mW cm^{-2}). A commercial $^1O_2$ indicator 9,10-anthracenediyl-bis(methylene)-dimalonic acid (ABDA) was used. ABDA can undergo oxidation by $^1O_2$ to yield endoperoxide, which results in a decrease of ABDA absorption. Under white light irradiation, the absorbance of ABDA solution in the presence of DCQu decreased dramatically with increasing irradiation time, and the ABDA was completely consumed in 6 min (Fig. 9A). From the changes of ABDA absorption, it was calculated that 16.99 nmol of ABDA was consumed upon light illumination for the initial 20 s. By contrast, three well-known and mostly used PSs, including Ce6, TPPS and Rose Bengal, with high $^1O_2$ generation efficiencies, only consumed 1.67, 2.69, and 3.04 nmol of ABDA under the same conditions, respectively. The $^1O_2$ generation ability of DCQu was determined to be 10.17, 6.32 and 5.59 times stronger than that of Ce6, TPPS and Rose Bengal, respectively (Fig. 9B). It is believed that the $^1O_2$ generation ability of DCQu is superior to that of previously reported AIE PSs.

In investigating the use of DCQu as a PS for PDT on living cells, white light irradiation-triggered ROS generation of DCQu inside HeLa cells was investigated. The HeLa cells were

incubated either with both H2DCF-DA and DCQu or with H2DCF-DA alone. As shown in Fig. 9C, an obvious increase in fluorescence signal was observed from the cells incubated with both H2DCF-DA and DCQu with increasing irradiation time, revealing efficient ROS generation from DCQu over the course of irradiation. In contrast, no obvious fluorescence increase was observed in the absence of DCQu (Fig. 10). To evaluate the therapeutic effect of DCQu under two-photon excitation, HeLa cells were incubated with DCQu and irradiated with 900 nm two-photon fs-laser scans. As shown in Fig. 9D, two-photon scans cause a gradual and significant change in cell morphology with increasing scan times. These changes are associated with cell necrosis and are apparently induced by $^1O_2$ generated by DCQu under two-photon excitation, revealing a great potential of DCQu for two-photon PDT.

Quantitative evaluation of the therapeutic effect of DCQu was studied by the standard MTT assay on HeLa cancer cells (Fig. 9E). Upon incubation of HeLa cells with DCQu in the dark, cell viability was still higher than 89% whatever the concentration of DCQu used (up to 10 μM), suggesting a low cytotoxicity of DCQu in dark conditions. However, with white light irradiation, DCQu displayed a remarkable dose-dependent toxicity reflected by the gradual decrease of cell viability (down to 9% at a concentration of 10×10^{-6} M), revealing a promising potential of DCQu in cancer cell ablation through photodynamic process.

In order to further verify the selectivity of DCQu in killing cancer cells over normal cells, evaluation of dose-dependent cytotoxicity was conducted under the same conditions employing HLF cells as a normal cell model. As a result, it was found that DCQu displays a negligible dark cytotoxicity on HLF cells similar to that of HeLa cells. Under white light irradiation, however, HLF cell viability slightly decreased to 68% at a concentration of 10×10^{-6} M, revealing that DCQu was less destructive to normal cells than cancer cells due to comparatively more accumulation of DCQu in cancer cells. These results suggest that DCQu with cancer cell-specific staining and subsequent killing capability has great potential to serve as a PS for cancer theranostics.

DCQu demonstrated high $^1O_2$ generation efficiency, excellent photostability and biocompatibility, and efficient in vitro PDT effect, all of which make DCQu a promising PS for in vivo PDT applications. Since melanoma is the most dangerous form of skin and eye cancer and is also the most suitable cancer for PDT treatment, the mice tumor model of melanoma was used for evaluating in vivo PDT applications. Prior to the in vivo experiment, the in vitro

therapeutic effect of DCQu on B16 melanoma cells was evaluated and further compared with that of Ce6. As depicted in Fig. 9F, upon white light irradiation, a significant therapeutic effect was verified for DCQu, reflected by the gradual decrease in cell viability to 18% at the concentration of 5×10^{-6} M, at which 24% of cell viability was obtained for Ce6, revealing a much better therapeutic effect of DCQu than that of Ce6.

As for in vivo PDT, the regression efficacy in tumor growth was investigated to evaluate the therapeutic effect of DCQu (Fig. 11A). As presented in Figs. 11B and 11C, negligible inhibition of tumor growth was observed for the mice treated with light, Ce6 or DCQu alone, as compared with the control group, indicating that pure light irradiation or PS does not possess any antitumor effect. Obviously, compared to rapid tumor growth in the control group within 30 d, the commercial Ce6 can gradually inhibit tumor growth under light irradiation during 30 days of consecutive treatments, but the tumor still increased in terms of the relative tumor volume. In dramatic contrast, just three successive treatments of DCQu together with light irradiation effectively stopped the tumor growth trend and further treatments significantly shrank tumor size to a minimum value starting from day 24, which is even smaller than that on day 0. Remarkably, DCQu together with light irradiation achieved a high tumor inhibition rate of 85.51%, which is much higher than 62.31% for Ce6 (Fig. 11D). Impressively, in three parallel "DCQu + light" groups, two of them showed a complete ablation of tumor in the mice, indicating a complete cure of B16 melanoma in vivo (Fig. 12). These results demonstrate a much better therapeutic effect of DCQu than that of Ce6 in inhibiting tumor growth through the PDT process even with ultralow irradiation power of 4.2 mW cm^{-2}.

The mice survival percentages after PDT treatment are shown in Fig. 11E. The survival percentage of the control and the mice treated with light, Ce6 or DCQu alone fell rapidly after 9 days, and all the mice died after 24 days. In contrast, the survival percentage of "Ce6 + light"- or "DCQu + light"-treated mice remained 60% and 80%, respectively, after 45 days, indicating that the PDT using DCQu as a PS significantly prolonged the survival of the tumor-bearing mice and inhibited tumor growth (Fig. 11E). In order to further clarify the tumor inhibition performance of DCQu, the mice in all the groups were sacrificed at the end of treatment, and then the tumor tissues were sliced and stained by hematoxylin and eosin (H&E) for histopathological analysis (Fig. 11G). It was observed that the tumor tissue in the control group displayed compact tumor cells with an intact structure. No significant difference among control, light and PS groups was

detected, suggesting that the tumor tissue is not affected by pure light or PS. In the "DCQu + Light" group, the tumor tissue was no longer structurally integrated, and there were necrotic areas and numerous nuclear fragments, both of which were much less serious in the group treated with Ce6. Noteworthy, during the whole PDT treatment there was no obvious body weight change (Fig. 11F) and pathological abnormality for main organs after H&E staining (Fig. 13) in the mice that were administered with DCQu compared to those of control groups, further corroborating the negligible toxic effect and excellent biocompatibility of DCQu as well as its effective use in PDT treatment.

The present subject matter being thus described, it will be apparent that the same may be modified or varied in many ways. Such modifications and variations are not to be regarded as a departure from the spirit and scope of the present subject matter, and all such modifications and variations are intended to be included within the scope of the following claims.

We Claim:

1. A fluorescent probe, comprising a compound having the following backbone structural formula:

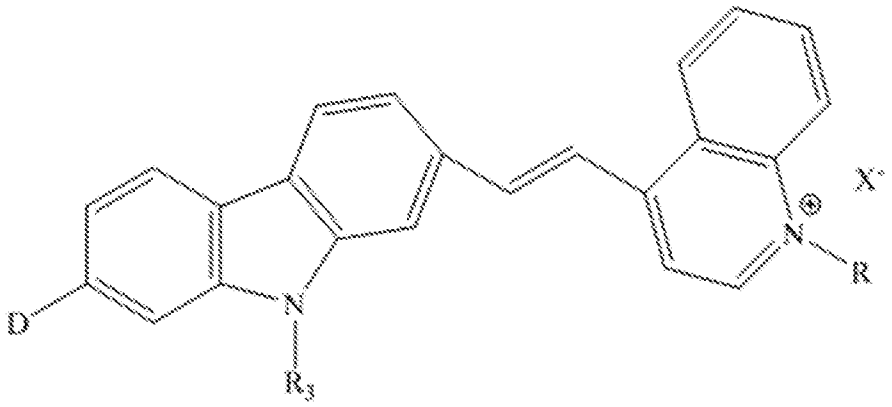

wherein each of R and R_3 is independently selected from the group consisting of H, alkyl, unsaturated alkyl, heteroalkyl, cycloalkyl, heterocycloalkyl, aryl, heteroaryl, alkoxy, alkyl-NCS, alkyl-N_3, and alkyl-NH_2;

X^- is selected from the group consisting of PF_6^-, BF_4^-, SbF_5^-, CH_3COO^-, CF_3COO^-, CO_3^{2-}, SO_4^{2-}, SO_3^{2-}, $CF_3SO_2^-$, TsO^-, ClO_4^-, F^-, Cl^-, Br^-, I^-, $(F_3CSO_2)N^-$, and PO_4^{3-};

D is selected from the group consisting of

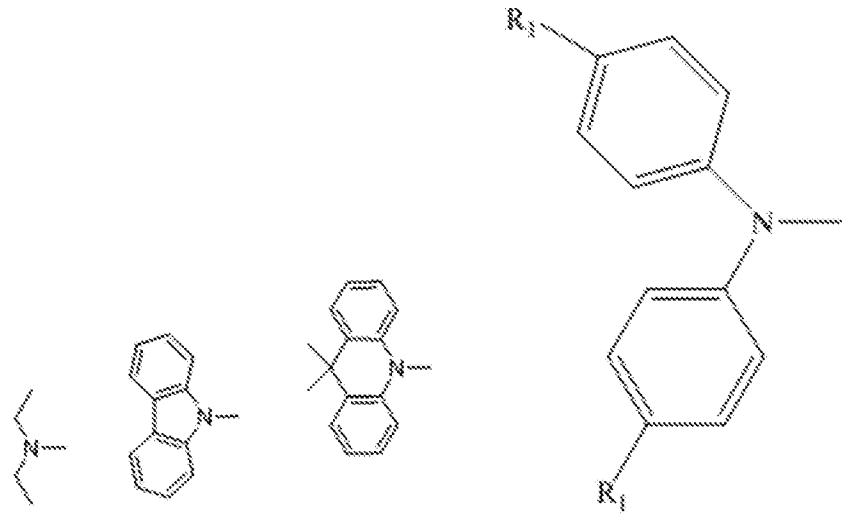

, and

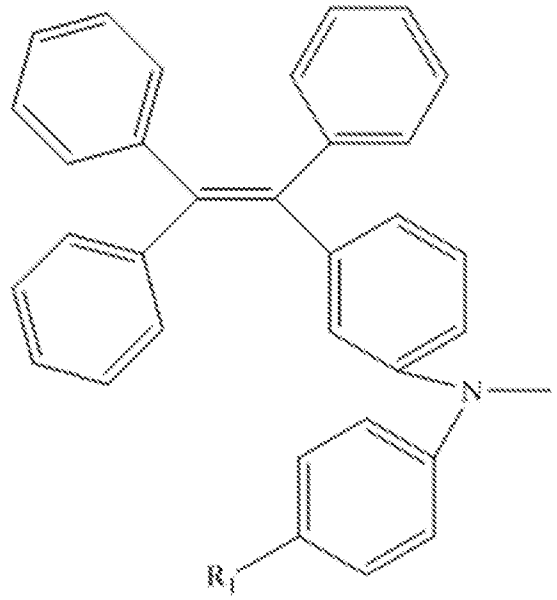

; and

each R_1 is independently selected from the group consisting of H, alkyl, unsaturated alkyl, heteroalkyl, cycloalkyl, heterocycloalkyl, aryl, heteroaryl, alkoxy, alkyl-NCS, alkyl-N_3, and alkyl-NH_2.

2. The probe according to claim 1, wherein the backbone structural formula is selected from the group consisting of

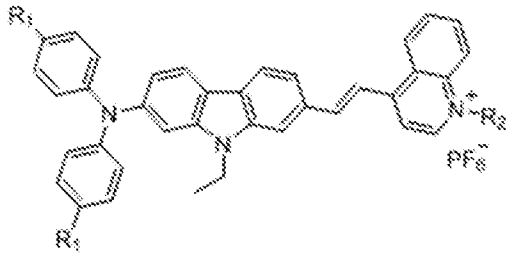

and

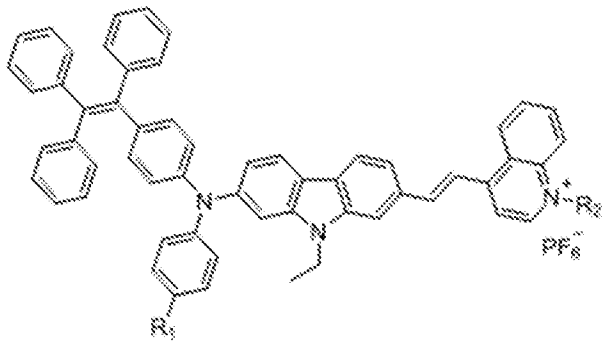

,

wherein each of R_1 and R_2 is independently selected from the group consisting of H, alkyl, unsaturated alkyl, heteroalkyl, cycloalkyl, heterocycloalkyl, aryl, heteroaryl, alkoxy, alkyl-NCS, alkyl-N_3, and alkyl-NH_2.

3. The probe of claim 2, wherein the compound is

is:

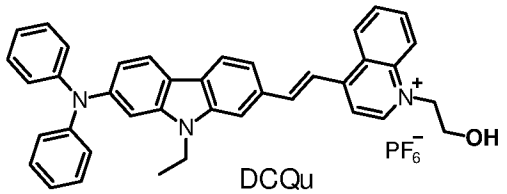

.

4. A method of cellular imaging, comprising:

contacting a target cell with the compound of claim 1, and

identifying a cellular target of interest using an imaging method.

5. The method of claim 4, wherein the imaging method is selected from the group consisting of fluorescence microscopy and confocal laser scanning microscopy.

6. The method of claim 5, wherein the fluorescence microscopy comprises two-photon excitation microscopy.

7. The method of cellular imaging according to claim 5, wherein the fluorescence microscopy comprises one-photon excitation microscopy.

8. The method of claim 4, wherein the target of interest comprises a mitochondrion.

9. A method of generating singlet oxygen, comprising irradiating the compound of claim 1 with white light.

10. A method of killing cancer cells, comprising:

contacting a target cancer cell with the compound of claim 1;

imaging the target cancer cell while the compound contacts the target cancer cell using an imaging method; and

subjecting the target cancer cell to white light irradiation while the compound is contacting the target cancer cell to kill the target cancer cell.

11. The method of claim 10, wherein subjecting the target cancer cell to white light irradiation comprises using an ultralow-power lamp having an irradiation power of about 4.2 mW cm^{-2}.

12. The method of claim 10, wherein the target cancer cell is within a living animal.

13. The method of claim 10, wherein the target cancer cell is a melanoma cancer cell.

14. A fluorescent probe comprising a compound have a backbone structural formula selected from the group consisting of

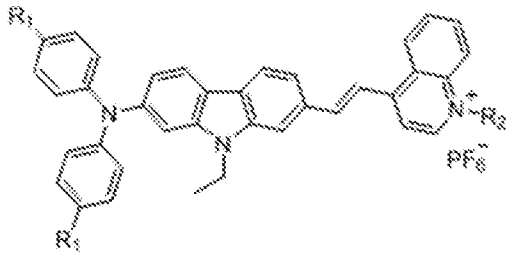

and

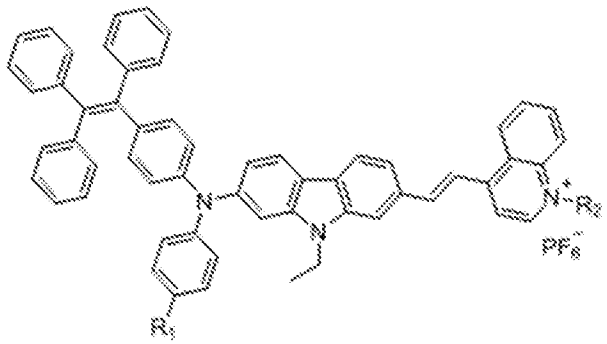

,

wherein each of R_1 and R_2 is independently selected from the group consisting of H, alkyl, unsaturated alkyl, heteroalkyl, cycloalkyl, heterocycloalkyl, aryl, heteroaryl, alkoxy, alkyl-NCS, alkyl-N_3, and alkyl-NH_2.

15. The probe of claim 14, wherein the compound is

is:

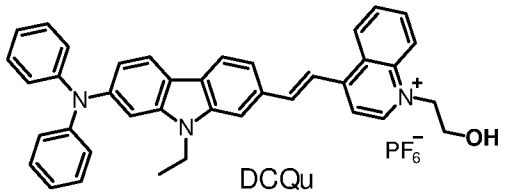

.

16. A method of cellular imaging, comprising:
contacting a target cell with the compound of claim 14, and
identifying a cellular target of interest using an imaging method.

17. The method of claim 16, wherein the imaging method is selected from the group consisting of fluorescence microscopy and confocal laser scanning microscopy.

18. The method of claim 16, wherein the fluorescence microscopy comprises two-photon excitation microscopy.

19. The method of claim 17, wherein the fluorescence microscopy comprises one-photon

excitation microscopy.

20. A method of killing cancer cells, comprising:

contacting a target cancer cell with the compound of claim 14;

imaging the target cancer cell while the compound contacts the target cancer cell using an imaging method; and

subjecting the target cancer cell to white light irradiation while the compound is contacting the target cancer cell to kill the target cancer cell.

Fig. 1A Fig. 1B Fig. 1C

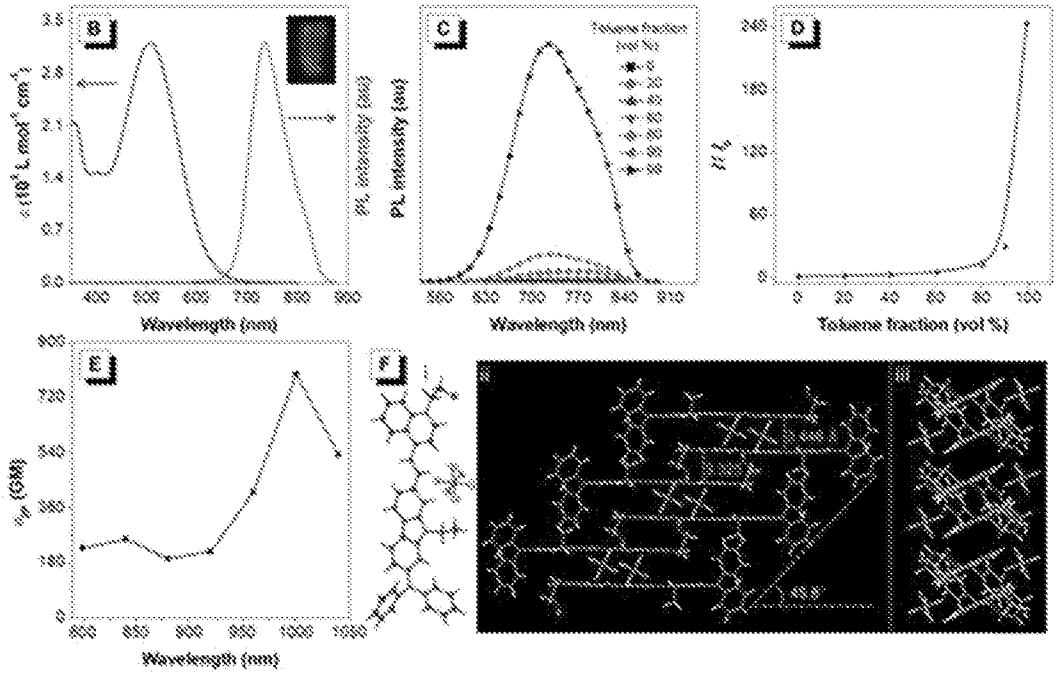

Fig. 1D Fig. 1E

FIGs. 1A-1E

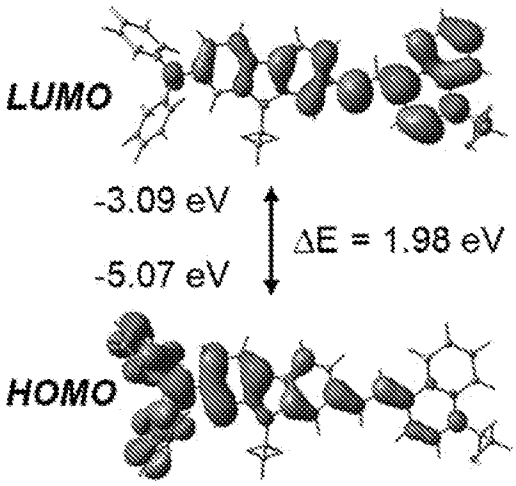

FIG. 2

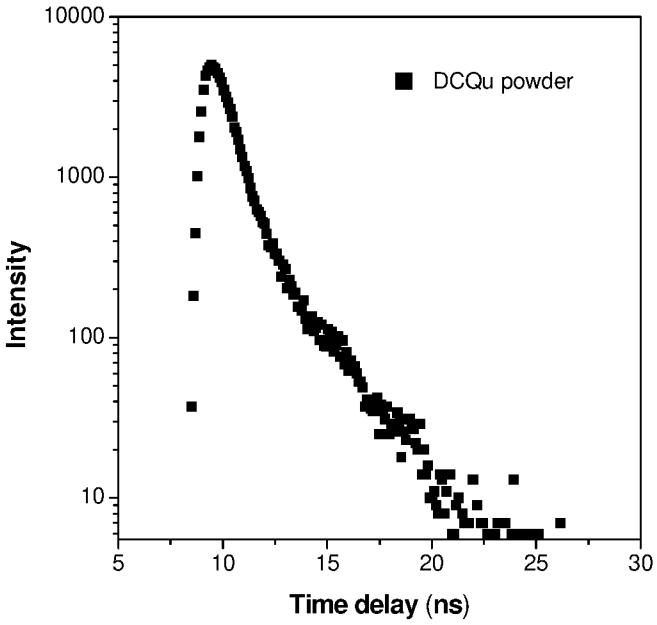
10000
1000
100
10
Intensity
DCQu powder
5
10
15
20
25
30
Time delay (ns)

FIG. 3

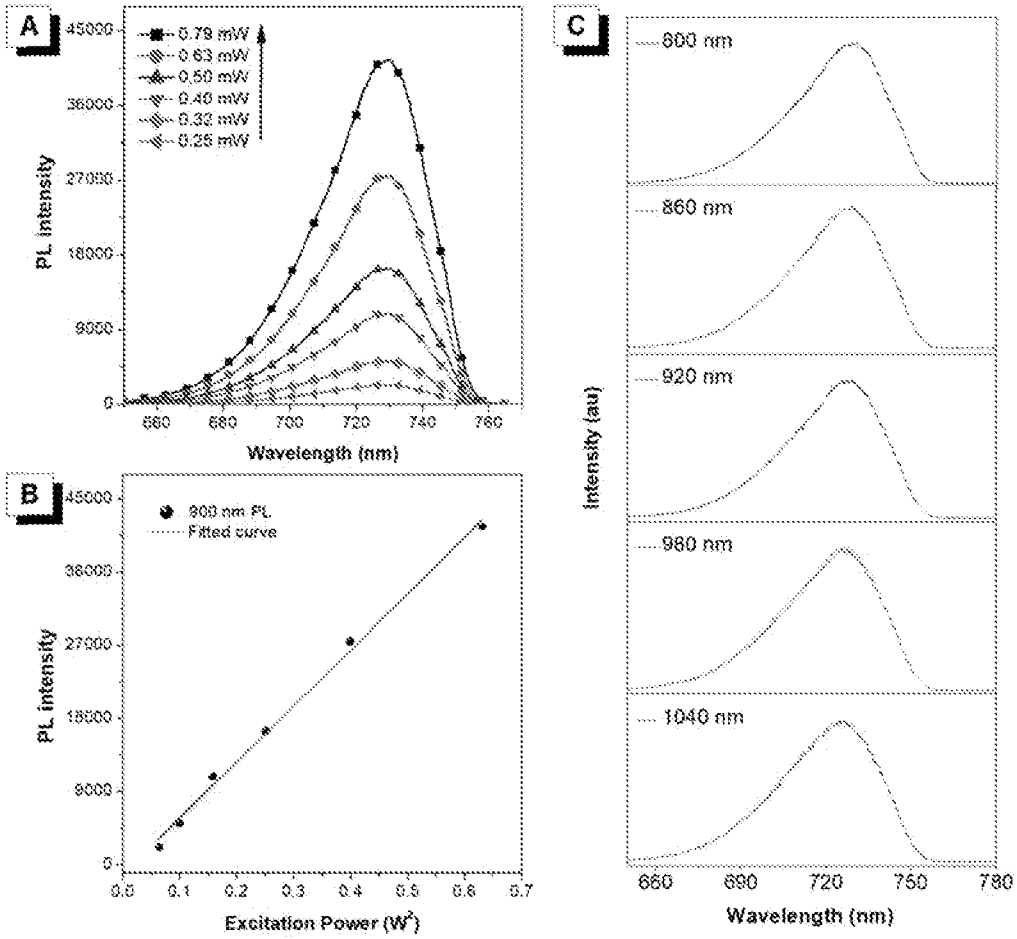
A
0.79 mW
0.63 mW
0.50 mW
0.40 mW
0.32 mW
0.25 mW
PL intensity
Wavelength (nm)
B
800 nm PL
Fitted curve
PL intensity
Excitation Power (W²)
C
800 nm
860 nm
920 nm
980 nm
1040 nm
Intensity (au)
Wavelength (nm)

FIGs. 4A-4C

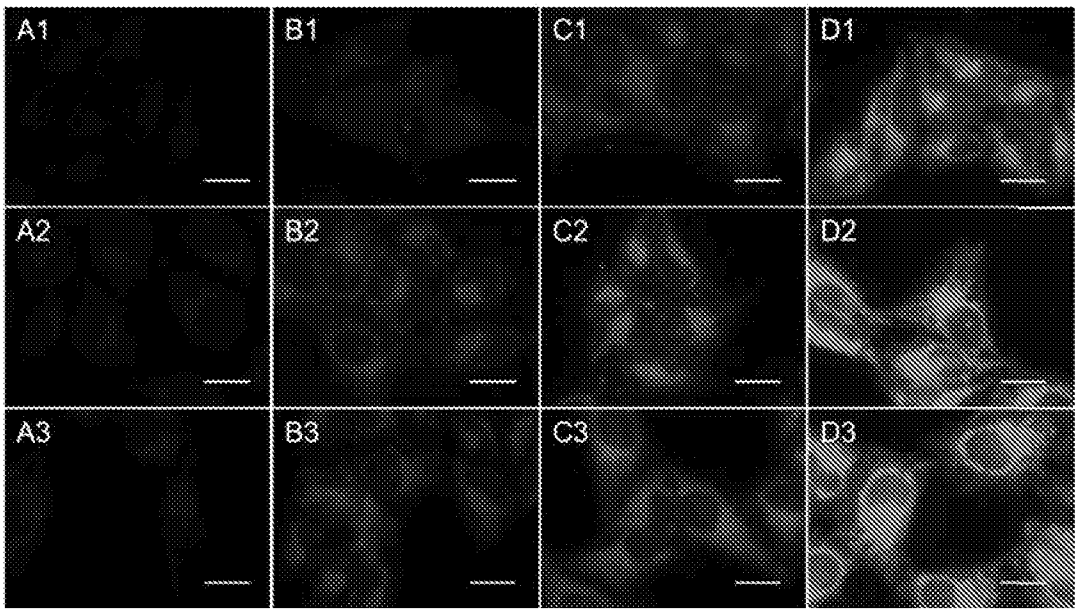

FIGs. 5A-5D

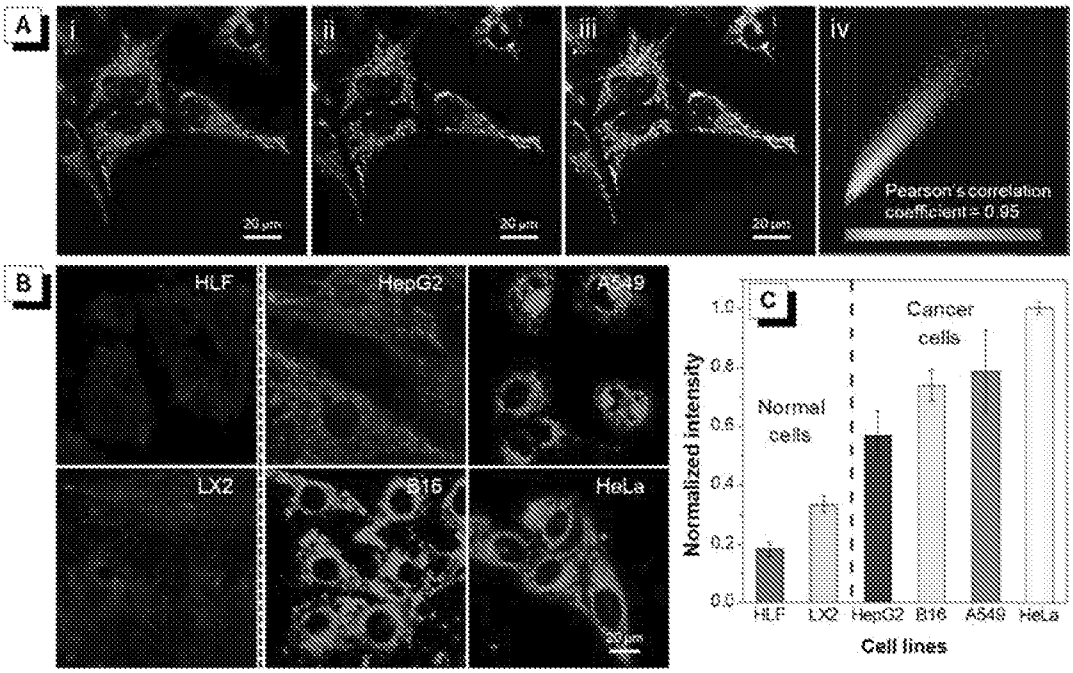

FIGs. 6A-6C

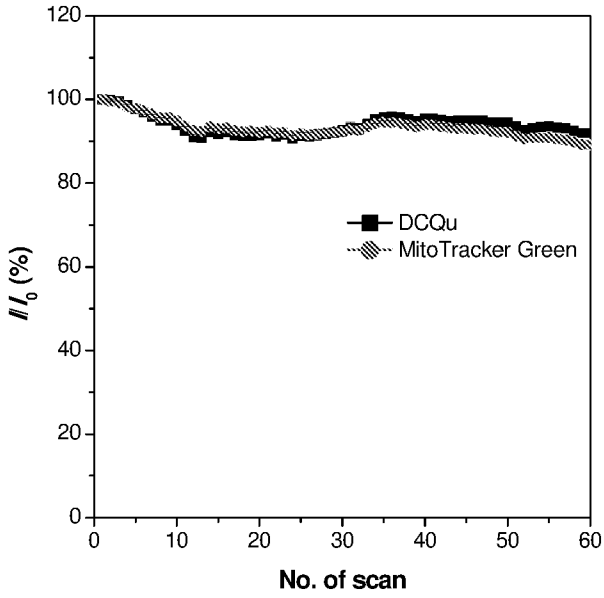

FIG. 7

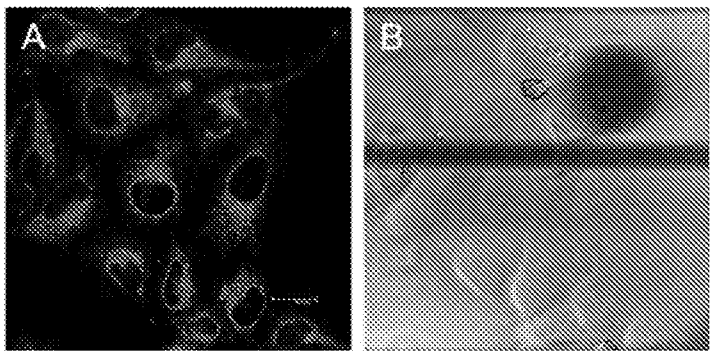

FIGs. 8A-8B

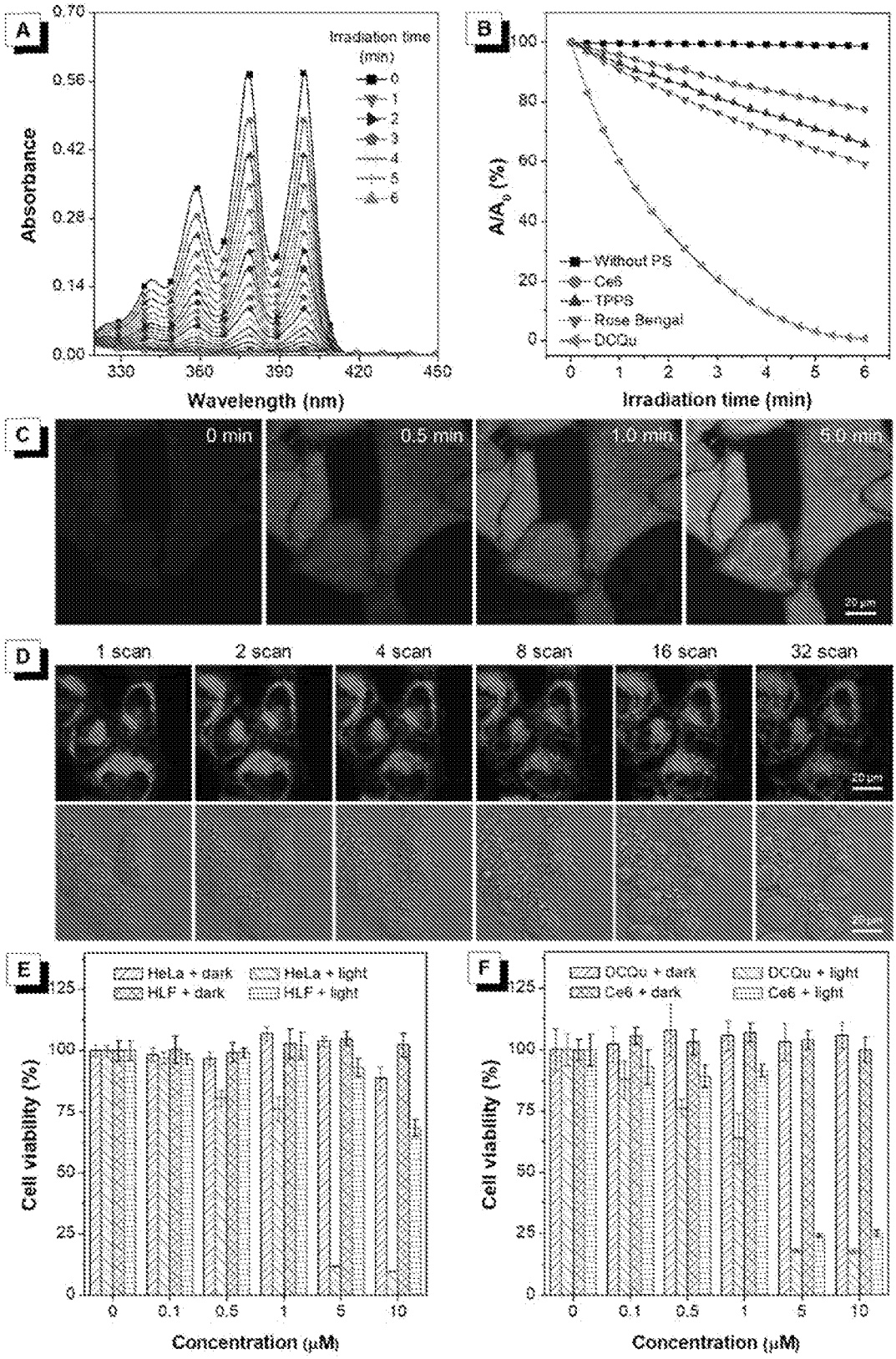
A
Absorbance
Wavelength (nm)
Irradiation time (min)
0
1
2
3
4
5
6
B
A/A0 (%)
Irradiation time (min)
Without PS
Ce6
TPPS
Rose Bengal
DCQu
C
0 min
0.5 min
1.0 min
5.0 min
D
1 scan
2 scan
4 scan
8 scan
16 scan
32 scan
E
HeLa + dark
HeLa + light
HLF + dark
HLF + light
Cell viability (%)
Concentration (μM)
F
DCQu + dark
DCQu + light
Ce6 + dark
Ce6 + light
Cell viability (%)
Concentration (μM)

Figs. 9A-9F

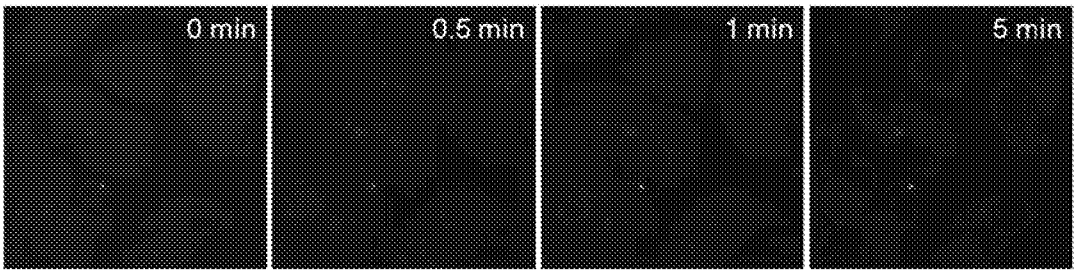

FIG. 10

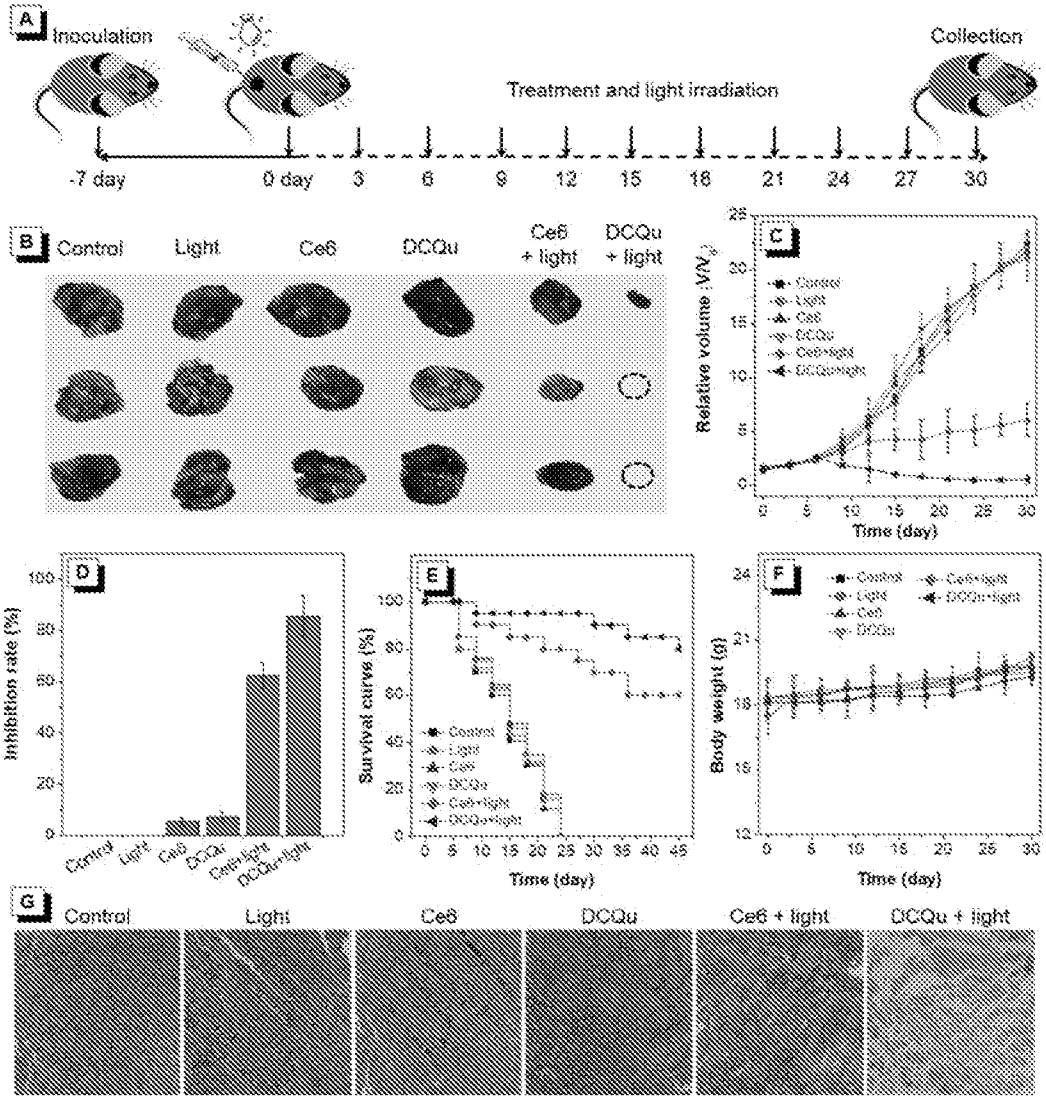
A
Inoculation
Collection
Treatment and light irradiation
-7 day
0 day
3
6
9
12
15
18
21
24
27
30
B
Control
Light
Ce6
DCQu
Ce6 + light
DCQu + light
C
Relative volume (V/V0)
Time (day)
D
Inhibition rate (%)
E
Survival curves (%)
Time (day)
F
Body weight (g)
Time (day)
G
Control
Light
Ce6
DCQu
Ce6 + light
DCQu + light

FIGs. 11A-11G

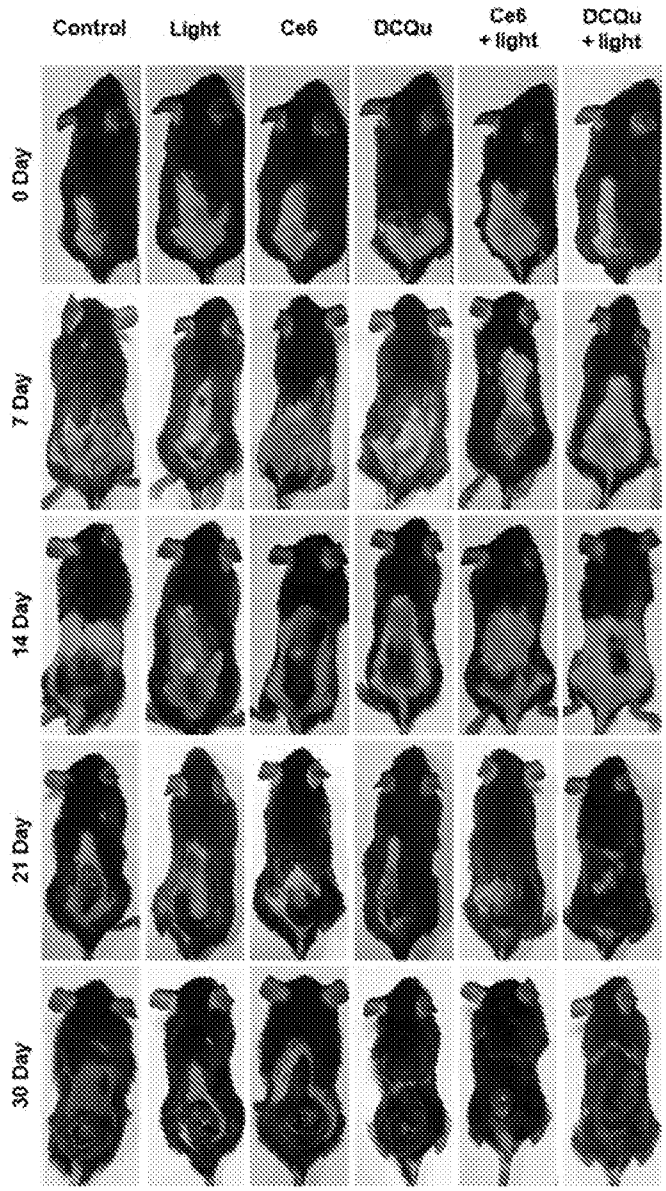
Control
Light
Ce6
DCQu
Ce6 + light
DCQu + light
0 Day
7 Day
14 Day
21 Day
30 Day

FIG. 12

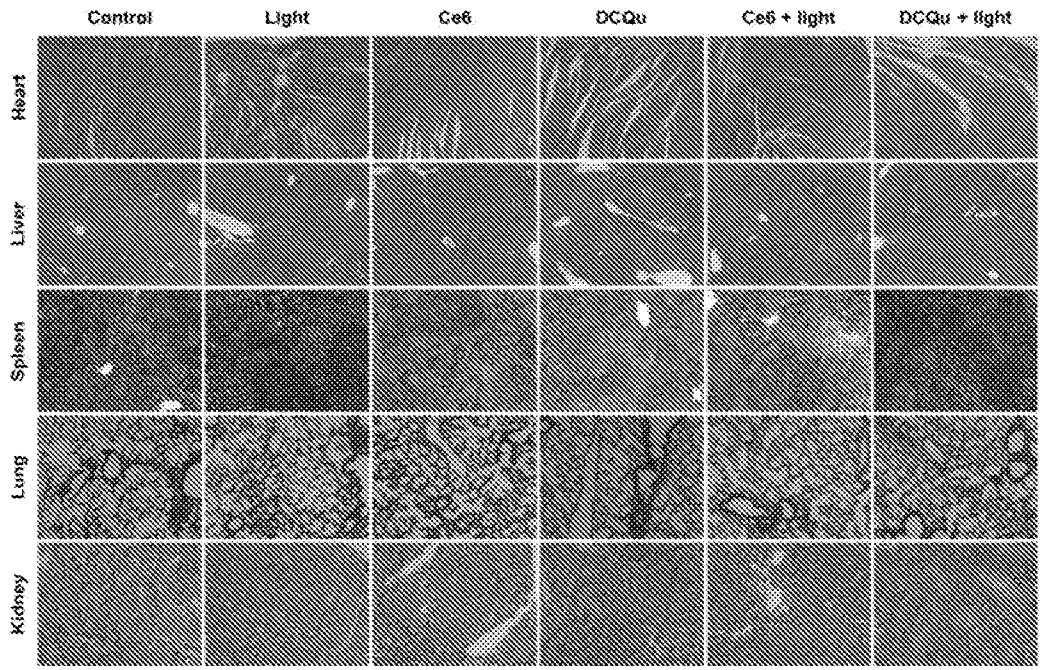
Control
Light
Ce6
DCQu
Ce6 + light
DCQu + light
Heart
Liver
Spleen
Lung
Kidney

Fig. 13

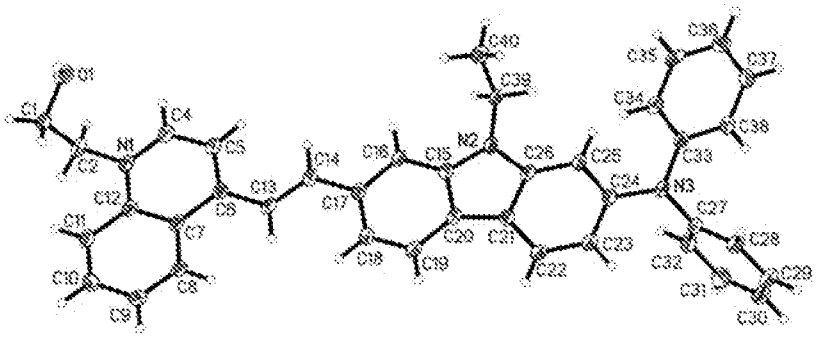
O1
C1
C2
N1
C4
C5
C12
C11
C10
C6
C7
C8
C9
C13
C14
C17
C16
C15
N2
C40
C39
C26
C25
C24
N3
C27
C28
C29
C30
C31
C32
C33
C34
C35
C36
C37
C38
C18
C19
C20
C21
C22
C23

FIG. 14

INTERNATIONAL SEARCH REPORT

International application No.
PCT/CN2020/074577

A. CLASSIFICATION OF SUBJECT MATTER

C07D 215/06(2006.01)i; C07D 209/82(2006.01)i; C07D 209/88(2006.01)i; C07D 401/06(2006.01)i; A61K 41/00(2020.01)i; A61K 49/00(2006.01)i; A61P 35/00(2006.01)i

According to International Patent Classification (IPC) or to both national classification and IPC

B. FIELDS SEARCHED

Minimum documentation searched (classification system followed by classification symbols)

C07D; A61K; A61P

Documentation searched other than minimum documentation to the extent that such documents are included in the fields searched

Electronic data base consulted during the international search (name of data base and, where practicable, search terms used)

CNABS,CNPAT,WPI,CNTXT,USTXT,EPTXT,WOTXT,ISI web of knowledge,STN: fluorescent probe, pyridine, carbazole, cellular imag+,cancer.

C. DOCUMENTS CONSIDERED TO BE RELEVANT

Category*	Citation of document, with indication, where appropriate, of the relevant passages	Relevant to claim No.
X	Zheng, Z.et al. "Bright Near-Infrared Aggregation-Induced Emission Luminogens with Strong Two-Photon Absorption, Excellent Organelle Specificity, and Efficient Photodynamic Therapy Potential" *ACS Nano,* Vol. 12, No. 8, 03 August 2018 (2018-08-03), pages 8145-8159	1-20
A	WO 2013030737 A1 (PIANETA S.R.L et al.) 07 March 2013 (2013-03-07) claims 1-13	1-20
A	JP 04101153 A (SHARP KK) 02 April 1992 (1992-04-02) claims 1-3	1-20
A	CN 102154003 A (天津城市建设学院) 17 August 2011 (2011-08-17) claims 1-4	1-20
A	Wei, Z.C. et al. "The effects of donor acceptor end groups of heterocyclic molecules on two-photon absorption properties" *Journal of Molecular Structure,* Vol. 748, 12 April 2005 (2005-04-12), pages 1-4	1-20

☐ Further documents are listed in the continuation of Box C. ☑ See patent family annex.

* Special categories of cited documents:
"A" document defining the general state of the art which is not considered to be of particular relevance
"E" earlier application or patent but published on or after the international filing date
"L" document which may throw doubts on priority claim(s) or which is cited to establish the publication date of another citation or other special reason (as specified)
"O" document referring to an oral disclosure, use, exhibition or other means
"P" document published prior to the international filing date but later than the priority date claimed
"T" later document published after the international filing date or priority date and not in conflict with the application but cited to understand the principle or theory underlying the invention
"X" document of particular relevance; the claimed invention cannot be considered novel or cannot be considered to involve an inventive step when the document is taken alone
"Y" document of particular relevance; the claimed invention cannot be considered to involve an inventive step when the document is combined with one or more other such documents, such combination being obvious to a person skilled in the art
"&" document member of the same patent family

Date of the actual completion of the international search	Date of mailing of the international search report
14 April 2020	**09 May 2020**
Name and mailing address of the ISA/CN **National Intellectual Property Administration, PRC** **6, Xitucheng Rd., Jimen Bridge, Haidian District, Beijing 100088** **China** Facsimile No. **(86-10)62019451**	Authorized officer **WU,Hongxia** Telephone No. **86-(10)-53962143**

INTERNATIONAL SEARCH REPORT

International application No.
PCT/CN2020/074577

Box No. II Observations where certain claims were found unsearchable (Continuation of item 2 of first sheet)

This international search report has not been established in respect of certain claims under Article 17(2)(a) for the following reasons:

1. ☑ Claims Nos.: **10-13,20**
because they relate to subject matter not required to be searched by this Authority, namely:

[1] Claims 10-13, 20 are directed to a method of treatment of the human/animal body. The report is based on the following subject matter: non-human/animal treatment method or non-treatment method.

2. ☐ Claims Nos.:
because they relate to parts of the international application that do not comply with the prescribed requirements to such an extent that no meaningful international search can be carried out, specifically:

3. ☐ Claims Nos.:
because they are dependent claims and are not drafted in accordance with the second and third sentences of Rule 6.4(a).

INTERNATIONAL SEARCH REPORT
Information on patent family members

International application No.
PCT/CN2020/074577

Patent document cited in search report			Publication date (day/month/year)	Patent family member(s)			Publication date (day/month/year)
WO	2013030737	A1	07 March 2013	IT	TO20110778	A1	27 February 2013
				EP	2748264	A1	02 July 2014
				US	2014246094	A1	04 September 2014
JP	04101153	A	02 April 1992	JP	H04101153	A	02 April 1992
CN	102154003	A	17 August 2011	CN	102154003	B	22 April 2015